



# **Gharyan Journal of Technolgy**

**Annual, Corrected and Accademic Journal**

**Issued By**

**Higher Institute of Sciences and Technology, Gharyan**

**Gharyan - Libya**

**Issue (7), July- 2021**

**International Code: ISSN (Print) 2518-5993**

**ISSN (Online) 2521-9308**

**[www.git.scitech-gh.edu.ly](http://www.git.scitech-gh.edu.ly)**



**Gharyan Journal of Technology**  
**Annual, Reviewed and Academic Journal**  
**Issued By :**  
**Higher Institute of Sciences and Technology, Gharyan**

<b>Dr: Melod Mohammed Unis</b>	<b>General Supervision</b>
<b>Dr:Ahmad Ramadan Kobaiz</b>	<b>Editor In Chief</b>
<b>Prof:Abdelati Elalem</b>	<b>Managing Editor</b>
<b>Mr: Mohamed Rajab Baiod</b>	<b>Member</b>
<b>Mr:Mohamed M.Alghiryani</b>	<b>Member</b>
<b>Mr:Abdulbasit Mohamad Ali</b>	<b>Member</b>

**Contact Us:**

**: Telephone 0913506053**  
**E-mail: ghjt2016 @ gmail.com**

## Contents

English Research Papers	Page
<b>Travel Time and Cost are Represents the Main Factors for Shifting Travel Mode Policy in Gharian Streets</b> Adel Ettaieb Elmloshi & Mohammed Mustafa Khalifa	4
<b>Waxy crude oil transportation in Gulf-sirt offshore field.</b> Melod M. Unis, Mohamed M. Alghiryani, Shada Alem	17
<b>Estimation of cementation factor for a field of around Brack sandstone Reservoir</b> Khaled taleb, Hakim Shebbani, Abduraof. A.Al amari.	33
<b>Analyzing and Modeling the Separation Distance of Lightning Arresters for 400kv Transfer Substation's Protection against the Lightning Strokes</b> Imhimmad Abood, Ahmed altawwary and Abdhakeem Alkwash	45
<b>Reversible Blind Image Watermarking based on Integer Wavelet Transform</b> Abdulmawla Najih, Salem Enajeh, Nabila Albannai	63

الصفحة	الأوراق البحثية باللغة العربية
11	أثر المحافظ الاستثمارية على ربحية المصارف الإسلامية الأردنية خالد ابو النور حسين ابراهيم، خالد محمد أحمد التونسي
32	أثر التضخم وسعر الصرف في الأداء المالي للمصارف التجارية الليبية دراسة تطبيقية على مصرفي الجمهورية والتجارة والتنمية خلال الفترة 2003-2017م عمر محمد بشينه، محمد عقيل زائد

57	دور الإنتمان المصرفي في تنمية الإقتصاد الليبي خلال الفترة (2020-1995) صلاح الدين إنبية جمعة، هدى محمد أبوخريص
81	خفض الركام الخشن في الخلطة الخرسانية وتأثيره على مقاومة الضغط للخرسانة عواطف عثمان الطويل، خالد محمد عمرو، عبد العالي أبوبكر عمر، حسين علي بلقاسم، عصام عمران الأجنف
89	تطوير الخلايا الشمسية باستخدام تقنية النانو خيرية علي محمد المغربي
107	أثر مؤشرات المركز المالي للمصارف التجارية على قيمتها السوقية خلال الفترة 2015 2019 - مولود رمضان ابوخريص، فتحي جماعة الزغداني

## Travel Time and Cost are Represents the Main Factors for Shifting Travel Mode Policy in Gharian Streets

Adel Ettaieb Elmloshi & Mohammed Mustafa Khalifa

Department of Civil and Structural Engineering / Engineering Faculty of Gharian  
Adel.elmloshi@gu.edu.ly – adelelmloshi@gmail.com - Mohamajary@gmail.com

### المخلص:

وسائل النقل مهمة جدا للمسافرين بمدينة غريان لأداء أنشطتهم ورحلاتهم اليومية. ومن جهة ثانية فإن زيادة العدد الإجمالي للسيارات الخاصة ومركبات النقل الخاص أي (سيارات الأجرة والحافلات الصغيرة) على الطرق يزداد ويسبب العديد من المشاكل اليومية على الطرق مثل الازدحام والحوادث المرورية والتلوث الضوضائي. والهدف من هذا البحث هو دراسة أهم عاملين لتحويل للنقل العام، تم إجراء مسح استقصائي في مدينة غريان لدراسة الانخفاض المحتمل للسيارات الخاصة ووسائل النقل الخاص على الطرق من خلال الاستخدام الأمثل لنظام النقل العام المناسب (PT) من أجل الحد من مشاكل الازدحام المروري مثل التأخير في وقت السفر. وقد أجريت تحليلات حول العلاقة بين عدد من العوامل مثل وقت السفر وتكلفة السفر للإجابة على أسئلة البحث. و تم استخدام نموذج الانحدار اللوجستي لتحليل العوامل التي تؤثر على المستخدمين لتحويل رحلاتهم إلى بدائل النقل العام.

الكلمات الرئيسية: وقت السفر، تكلفة السفر، السيارات الخاصة، النقل العام(PT) ، الازدحام المروري والانحدار اللوجستي.

### ABSTRACT :

Transport modes are very important to Libyan's Gharian travellers for their activities and daily trips. However, the increase of total number of private car and private transport namely (taxi and micro buses) on the road increases and causes many road problems such as traffic congestion, accidents and noise pollution. The aim of this research is to study the two important factors to shifting to public transportation. Analyses about relation between factors as travel time and cost have been made to answer research questions. A questionnaire survey in Gharian city was carried out to study the potential reduction of private cars on road through optimal use of suitable public transportation system (PT) in order to reduce traffic congestion problems such as travel time. Logistic regression model has been used

to analyse the factors that influence users to shift their trips to public transportation alternatives.

**Key words:** travel time, travel cost, private car, public transport (PT), traffic congestion and Logistic regression.

## INTRODUCTION :

Private cars are important for most household activities in Libyan societies. They give comfort and convenience to the users to go to different destinations without affecting other users [4]. Private car is one of the important modes of personal transport in Libya cities, mainly because it is cheap and more reliable than the existing transport modes available namely (taxi and micro buses) [5]. Private car use has obvious negative effects, such as the traffic congestion, accidents and noise pollution. The shortage of private and public transportation services especially public buses in Gharian may be the reason why travellers prefer to use private cars [9]. In fact, in Gharian city there are many areas that do not have private transportation and acute shortage public transportation services. This situation encourages travellers in these areas to use private cars to make their daily trips. Increase in parking cost may cause private car users to think many times about their travelling behavior and travelling choices [1]. Finally, the shift will save their expenditure on transportation and may also reduce travel time and traffic congestion.

## STUDY PROBLEM :

The private Car is easily available vehicle in Libya [2]. Each Libyan household has owned one or more cars and they can travel by their private cars in a few minutes from place to another and most the people prefer the car because they can travel freely. Understanding travel behavior and the reasons for choosing one transport mode over another is an essential issue. However, travel behavior is more complex. For each trip, commuters have the choice between different modes of transportation. Each mode is having specific characteristics, such as advantages and disadvantages depended on travel time and parking cost [5]. Travellers in Gharian used private transport namely (microbuses, private taxis and coaches) and private cars to their works or study activities. Private transport can be owned and operated by individuals or company. The uncontrolled usage of these transport modes has caused road traffic congestion which has increased travel time, accident and pollution to the city environment [3]. Due to the complex scenarios happening

in Gharian city a study has been carried out to understand the travel behavior and try to establish suitable models to reasonably describe travellers' attitude and perception in the city.

## **DATA COLLECTION AND ANALYSIS :**

The understanding of travel behavior should be done through data collection [6]. The data collection was done through field study i.e. survey. The survey was done using questionnaires to get relevant data. The respondents for this survey are the private vehicles' users at study areas who use their private car and private transport as (taxi, minibuses) to make their different trips. The respondents were selected randomly [8]. The questionnaires were printed by Arabic language, to provide easier understanding and answering for some respondents. Respondents were selected randomly from travellers in study areas which does not have public transportation services. This survey was done on work days (Sunday to Thursday). The total number of respondents who was involved in this research was 170 respondents [8]. Excel software was used to analyse the questionnaire and also logistic regression method was used in this study.

## **DATA ANALYSIS OF TRAVEL TIME AND TRAVEL COST IN GHARIAN STREETS BY PRIVATE CAR AND PRIVATE TRANSPORT:**

This section describes survey results and the analysis of the data collected about the travellers of private car users used. Data was analysed by logistic regression models for probability prediction travelling behaviour in Gharian city streets, model for the private car for all types of trips, to determine the relationship between the two factors that influence the shift to public transport. The probability of private car drivers shifting to public transport is also examined based on travel cost, travel time.

### **Effect of Travel Cost on Travel Mode :**

Figure (1) as shows that 57% of the respondents paid less than 5 Libyan dinar (LyD) cost per trip, 28.9% paid about 6 to 10 LyD, 5.9% paid about 11 to 15 LyD, 8.1% paid more than 15 LyD.

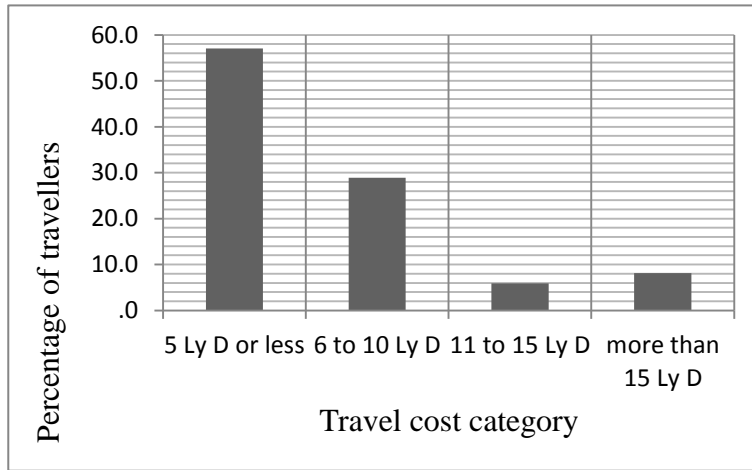


**Figure (1): Travel Cost for Trips**

The data of travel cost collected for this factor are shown in figure (1). The data are represented in the form of cumulative format in third column in Table (1), which shows the Travel cost category with respect to survey results and the probability of prediction (P) values. P value is derived from Equation (1) which involves constant and alpha ( $\alpha$ ) values to verify the logistic prediction model used in this study. This function has a continuous derivative, which allows it to be used in back propagation, according to Patterson [7]. The following functional form is used in this study to determine the shift probability of dependent variables.

$$P = \frac{1}{1+De^{\alpha(x)}} \quad \text{Equ. (1)}$$

Where,

P = prediction probability of shift to Public transportation (PT)

D = constant

$\alpha$  = coefficient of x

x = Category of travel cost

e = the base of natural logarithms (approximately 2.718)

**Table (1) Survey result and data calibration for travel cost category**

Category	Travel cost	Cumulative (P) Survey result	1-P	P/1-P	ln(P/1-P)
1	5 LyD or less	0.57	0.43	1.325581	0.281851
2	6 to 10 LyD	0.859	0.141	6.092199	1.807009
3	11 to 15 LyD	0.919	0.081	11.34568	2.428837



4	More than 15LyD	0.99	0.01	99	4.59512
---	-----------------	------	------	----	---------

The model shift probabilities were categorized by various categories of travel cost as shown in Figure (2). Mode shift probabilities ranged from 43% probability of private car use with travel cost (5 LyD or less) to 1% probability of private car use with travel cost (more than 15 LyD). In other words, public transport users probability increased from 57% with travel cost (5 LyD or less) to 99% of probability when travel cost (more than 15 LyD).

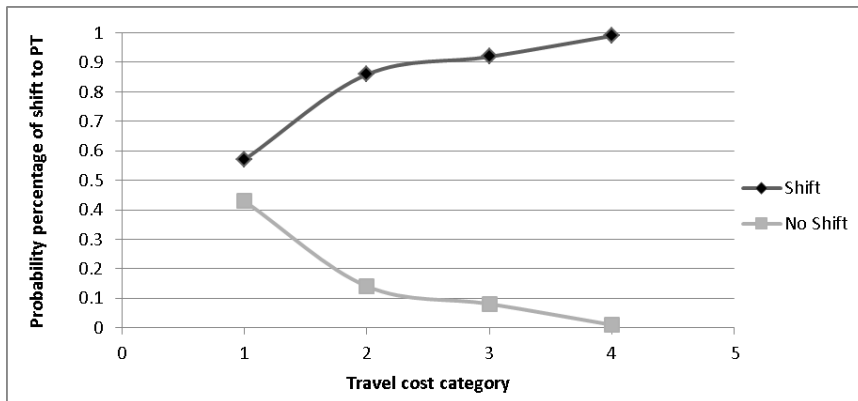


**Figure (2): Shifting percent - Travel cost category**

A simple linear regression analysis was then conducted by using Microsoft Excel to obtain the intercept constant (D) and the  $\alpha$  value. The results of the above Table (1) reflect the model calibration process which then introduced to excel to get the ANOVA table, which is described in Table (2), used to develop the Analysis of Variance (ANOVA) table which some important factors reflect the study significance that the values of R square, intercept coefficient and the important factor was alpha value which is used in the equation (1) above to verify the used model. By using the alpha ( $\alpha$ ) and (D) values from the ANOVA table, our model achieved the value of P equal to 0.021184 which is somehow acceptable to be significant (significant value is  $<0.05$ ) as shown in Equation (2).

**Table (2): The ANOVA table for travel cost category**

	Intercept	X Variable 1
Coefficients	-1.1122	1.356163
Standard Error	0.549324	0.200585
t Stat	-2.02468	6.761046
P-value	0.180186	0.021184
Lower 95%	-3.47576	0.493116
Upper 95%	1.251347	2.21921
Lower 95.0%	-3.47576	0.493116
Upper 95.0%	1.251347	2.21921

$$\ln D = -1.1122 \quad D = 3.041054$$

$$\alpha = 1.356163$$

$$R^2 = 0.9581$$

Where  $R^2$  approaches one value indicating the model's strong correlation power thus, the result of the prediction models can be as shown in Table (3) and Figure (3)

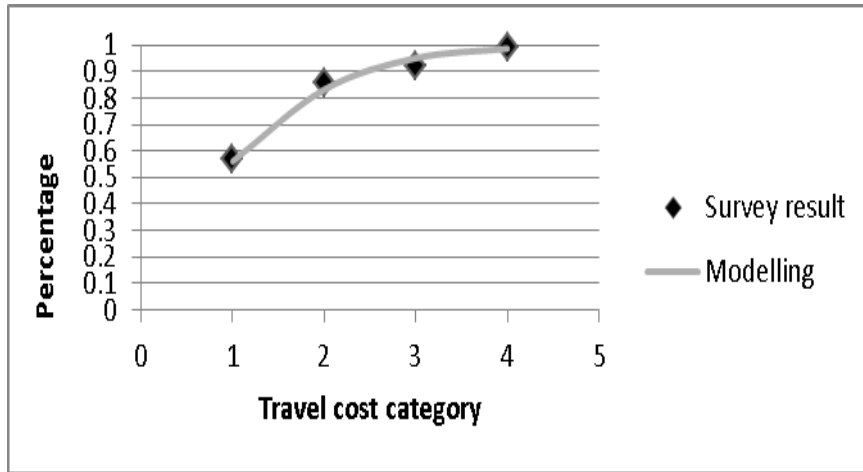
$$P = \frac{1}{1+3.041054e^{1.356163(x)}} \quad \text{Equ. (2)}$$

Table (3) shows the respective survey data and model data that correspond to the travel cost.

**Table (3): Survey result and logit model result for travel cost category**

Category	Travel cost	Cumulative (P) Survey result	Modelling result
1	5 LyD or less	0.57	0.561
2	6 to 10 LyD	0.859	0.832
3	11 to 15 LyD	0.919	0.951
4	More than 15LyD	0.99	0.9868

This result is more identified in Figure (3) which shows a high correlation between survey results and the modelled counterparts



**Figure (3): Correlation between survey results and modelling – Travel cost category**

#### Travel time for work to study trip by private car :

Figure (4) shows 41.5% respondents travelling daily from home to work or study in 10 minutes or less, 38.5% between 11 and 20 minutes, 14.1% between 21 and 30 minutes, 1.5% between 31 and 40 minutes, and 4.4% more than 40 minutes.

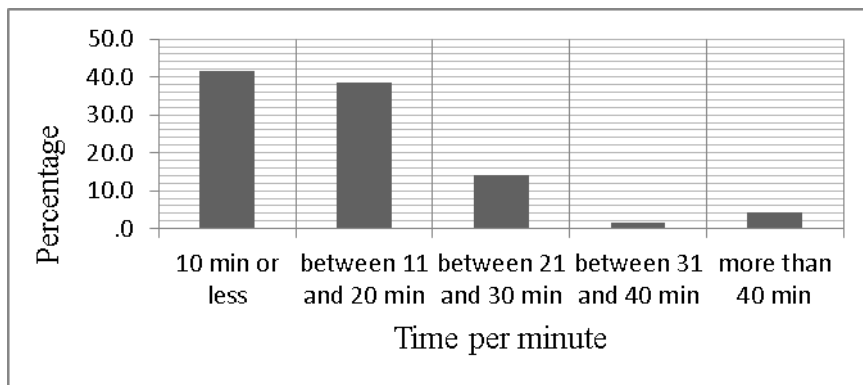


**Figure (4): Shows Travel Time**

The data of Travel time collected for this factor are shown in figure (4). The data are represented in the form of cumulative format in third column

in Table (4), which shows the Travel time category with respect to survey results and the probability of prediction (P) values. P value is derived from Equation (3) which involves constant and alpha ( $\alpha$ ) values to verify the logistic prediction model used in this study.

$$P = \frac{1}{1+De^{\alpha(x)}} \quad \text{Equ. (3)}$$

Where,

P = prediction probability of shift to PT

D = constant

$\alpha$  = coefficient of x

x = Category of travel time

e = the base of natural logarithms (approximately 2.718)

**Table (4) Survey result and data calibration for travel time category**

Category	Travel time	Cumulative (P) Survey result	1-P	P/1-P	ln(P/1-P)
1	10 min or less	0.415	0.585	0.709402	-0.34333
2	11 to 20 min	0.8	0.2	4	1.386294
3	21 to 30 min	0.941	0.059	15.94915	2.769406
4	31 to 40 min	0.956	0.044	21.72727	3.078568
5	More than 40 min	0.99	0.01	99	4.59512

The model shift probabilities were categorized by various categories of travel time shown in Figure (5). Mode shift probabilities ranged from 58.5% probability of private car use with travel time 10 minutes or less to 1% probability of private car use with travel time more than 40 minute. In other words, the probabilities of public transport user increased from 41.5% at travel time 10 minutes or less to 99% of probability with a travel time more than 40 minute.

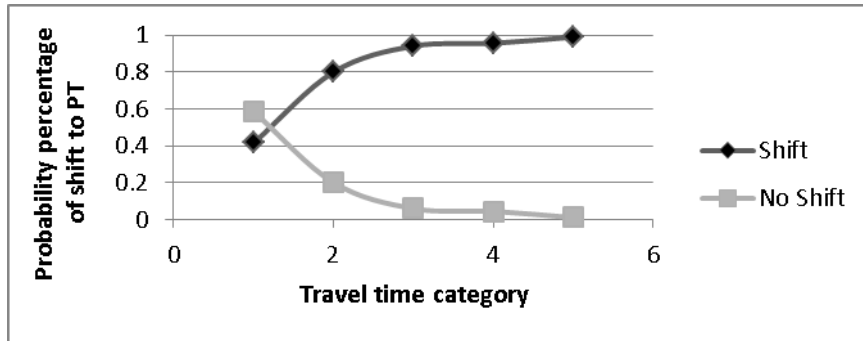


**Figure (5): Shifting percent - Travel time category**

A simple linear regression analysis was then conducted by using Microsoft Excel to obtain the intercept constant (D) and the  $\alpha$  value. The results of the above Table (4) reflect the model calibration process which then introduced to excel to get the ANOVA table, which is described in Table (5), uses to develop the Analysis of Variance (ANOVA) table which some important factors reflect the study significant which is the values of R square, intercept coefficient and the important factor was alpha value which is used in the equation (3) above to verify the used model. By using the alpha ( $\alpha$ ) and (D) values from the ANOVA table, our model achieved the value of P equal to 0.003205 which is somehow acceptable to be significant (significant value is  $<0.05$ ) as shown in Equation (4).

**Table (5): The ANOVA table for travel time category**

	Intercept	X Variable 1
Coefficients	-1.17354	1.156918
Standard Error	0.441465	0.133107
t Stat	-2.65829	8.691654
P-value	0.07645	0.003205
Lower 95%	-2.57848	0.733313
Upper 95%	0.231396	1.580523
Lower 95.0%	-2.57848	0.733313
Upper 95.0%	0.231396	1.580523

$$\ln D = -1.17354 \quad D = 3.233429$$

$$\alpha = 1.156918$$

$$R^2 = 0.961805$$

Where R2 approaches one value indicating the model's strong correlation power thus, the result of the prediction models can be as shown in Table (6) and Figure (6)

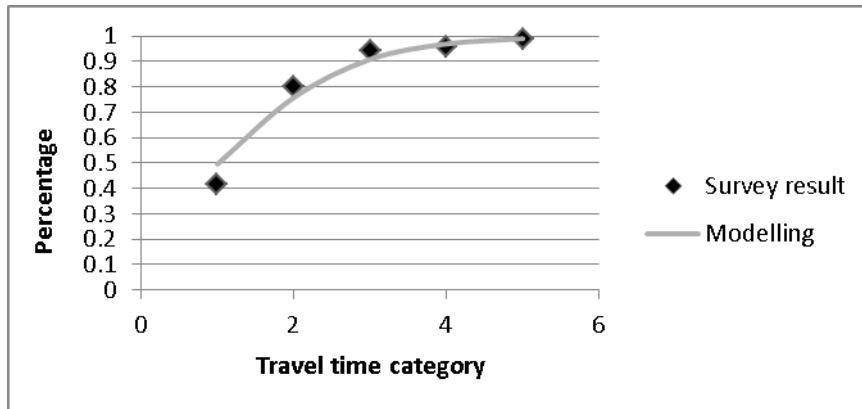
$$P = \frac{1}{1+3.233429e^{1.156918(x)}} \quad \text{Equ. (4)}$$

Table (6) shows the respective survey data and model data that correspond to the travel time.

**Table (6) Survey result and logit model result for travel time category**

Category	Travel time	Cumulative (P) Survey result	Modelling result
1	10 min or less	0.415	0.495844
2	11 to 20 min	0.8	0.757733
3	21 to 30 min	0.941	0.908646
4	31 to 40 min	0.956	0.969354
5	More than 40 min	0.99	0.990156

This result is more identified in Figure (6) which shows a high correlation between survey results and the modelled counterparts.



**Figure (6): Correlation between survey results and modelling – Travel time category**

## DISCUSSION :

This study has also revealed that positive and negative operations are needed to encourage travellers to shift from private car and private transport to public transport. The positive operation would be to reduce travel time, cost and improve service (more frequent and more on-time trips), and the negative operation for example if increases the parking fees and reduce number of the parking spaces in the city. The collected data were obtained from our survey which was subjected to the logistic model prior to the calibration process.  $D$  and  $\alpha$  value were extracted to be used in our model equation. Then the validation process took place to fit our results into the model. From the ANOVA results, the value of  $R$  square was within the normal range. Based on the given results, our model was approximately significant with the  $P$  value of  $< 0.05$ . Results of the study have shown that more time will be used to travel by private car and private transport for work or study trips, and these scenarios have encouraged the travellers to shift to the public transport (PT) system. The logistic regression applied depending on the factors affecting the shift from car to public transport (Travel cost, Travel time). These factors have encouraged the travellers to shift to the public transport (PT) system. About the travel cost, public transport users probability increased from 57% with travel cost (5 LyD or less) to 99% of probability when travel cost (more than 15 LyD). For travel time, the probabilities of public transport user increased from 41.5% at travel time (10 minutes or less) to 99% of probability with a travel time (more than 40 minute).

## CONCLUSION :

The increasing number of private cars and private transport namely taxi, minibuses and coaches in Gharian city has been named as the cause for increased road traffic congestion, environmental pollution and traffic accidents. This study shows the need to introduce an efficient public transport (PT) system to reduce traffic problems such as traffic congestion,

road accidents and delay in travel time on Gharian roads network as have been reported for all trips. Gharian people need to cooperate and support the use of the public transport (PT) system. It is very important to relieve the traffic problems on Gharian streets. Finally, all these factors have spurred the shift from using private vehicles to using the public transport system for all travellers' trips for various purposes in their daily lives.

### **ACKNOWLEDEMENT :**

The research was conducted in collaboration with the Civil Engineering and Structural Department, Engineering Faculty of Gharian, Gharian University – Libya .

### **REFERENCES :**

- [1] Adel Ettaieb Elmloshi, Amiruddin Ismail: Main Factors to Encourage Switch to Public Transport System, Tripoli – Libya Regional Engineering Postgraduate Conference (EPC) 2011
- [2] Adel Ettaieb Elmloshi, Probabilities of Policy Shift to Public Transport, Case study: Tripoli – Libya. International Conference on Technical Sciences (ICST2019) March 2019 60 –40.
- [3] Alrabotti Fathi Bashir (2007) Traffic Lights, part two (Tripoli)
- [4] Amiruddin Ismail, Adel Ettaieb Elmloshi. Logistic Regression Models to Forecast Travelling Behaviour in Tripoli City Proceeding of the International Conference on Advanced Science, Engineering and Information Technology 2011.
- [5] Amiruddin Ismail#, Adel Ettaieb Elmloshi# Travel Time is the Main Factor for Switching Travel Mode in Tripoli Street: Proceedings of the Eastern Asia Society for Transportation Studies, Vol.8, 2011
- [6] El-Sayed Shawaly (1995). “In Search For Some Low-Cost Engineering Remedial Measures In Heavily Trafficked Corridors In El-Mansoura City “, First Engineering Conference, Mansoura University.
- [7] Patterson, Z.; Ewing, G. & Haider, M. 2005. Gender-based analysis of work trip mode choice of commuters in Suburban Montreal, Canada, with stated preference data. *Transportation Research Record* 1924: 85-93.



- [8] Sekaran, U. 2003. Research Methods For Business, A skill Building Approach, Fourth Edition. ISBN 978-0-471-20366-7.
- [9] Secretariat of the Libyan justice, general Traffic department-Office and licensing of Tripoli, data as of 2009 .

## Waxy crude oil transportation in Gulf-sirt offshore field.

Melod M. Unis<sup>1</sup>, Mohamed M. Alghiryani<sup>2</sup>, Shada Alem<sup>3</sup>

1,2- Higher Institute of Sciences And Technology, Gharyan. Libya,  
3- Chemical Engineering Department, Tripoli University Tripoli- Libya.

### المخلص :

يُذكر في هذه الورقة نقل النفط الخام في خطوط الانابيب التي تربط المنصات في مشروع خليج سرت البحري. حيث يؤدي ترسب الشمع (وهو في حالته الصلبة) في جدار الأنبوب الى حدوث خلل في الضغط والذي بدوره يسبب انسدادا اصطناعيا يؤدي الى انخفاض او انقطاع في الانتاج. حيث يمكن ان يترسب الشمع وهو في الحالة الصلبة على جدار الأنبوب عندما تنخفض درجة حرارته إلى درجة اقل، فيما يعرف (WAT).

يهدف هذا العمل الى دراسة عملية ترسيب الشمع على السطح الداخلي لأنابيب إنتاج النفط وتأثيره على معاملات مثل معدل التدفق، درجة حرارة جدار الأنبوب، خط الأنابيب المعزول، وتأثير تكوين النفط الخام ودرجات حرارة مياه البحر على سماكة الرواسب. تم إجراء التحليل على افتراض وجود محاكاة على طور المائع وتم تنفيذ ذلك عدديا باستخدام برمجة

.MATLAB

أظهرت النتائج ان زيادة معدلات التدفق تقلل من سماكة الرواسب القسوى، ومنع العزل المزيد من الترسبات الصلبة، كما أظهرت (WAT) أعلى سماكة أكثر للرواسب وانخفاض كمية المواد الصلبة المترسبة مع زيادة في درجة حرارة الزيت الخام او درجة حرارة مياه البحر حيث ينتشر على مسافة اطول في الانبوب معتبرين ان درجة حرارة الجدار ثابتة او تدرج حراري محوري مع ميل موجب، ويلاحظ التأثير المعاكس عند النظر الى التدرج الحراري المحوري ذي المنحدر السالب.

### Abstract:

Crude oil transportation in the pipe lines connecting platforms at projected offshore Gulf-Sirt project is assumed in this paper. The precipitation of the solid phase of wax in the pipe wall creates pressure abnormalities and causing an artificial blockages leading to a reduction or interruption in the production. Wax can precipitate as a solid phase on the pipe wall when its temperature drops below the appearance temperature (WAT).

This work is aimed to study the wax deposition process on the internal surface of oil production pipelines and the influence of parameters such as flow rate, pipe wall temperature, Insulated Pipeline, Effect of Crude-Oil Composition (or WAT), Effect of Crude-Oil and Seawater Temperatures on the deposit thickness.

The analysis was conducted assuming pseudo steady conditions on the fluid phase, the solution was implemented numerically using the MATLAB PROGRAMMING. The results showed that increased flow rates reduce the maximum deposit thickness, insulation preventing further solids deposition, The higher WAT gave a larger deposit thickness, reduction in the amount of deposited solids with an increase in either the crude-oil temperature or the seawater temperature, as it spreads on a longer distance in the pipe when considering a constant wall temperature or the axial thermal gradient with a positive slope, and the opposite effect is observed when considering the axial thermal gradient with a negative slope.

Key words : Waxy crude oil, MATLAB PROGRAMMING, wax deposition, crude oil transportation .

## **Introduction:**

When a liquid flowing through a pipeline is exposed to a cold environment that is below its freezing-point temperature (or solubility temperature), solids deposition on the pipe wall is likely to occur. This phenomenon takes place frequently during the transportation of “waxy” crude oils that contain high-molecular-weight alkanes or paraffin waxes. Paraffin waxes have a reduced solubility in crude oils at lower temperatures, causing their crystallization and deposition on cooler surfaces.

The adverse effects of wax deposition are encountered in all sectors of the petroleum industry, ranging from oil reservoir formations to blockage of pipelines and process equipment. The deposited wax impedes the flow of oil through the pipeline, causing an increase in the pumping power. If not

controlled adequately, the deposited solids may block the pipeline, resulting in high costs for its cleaning. Remediation can be carried out using mechanical cleaning methods, chemical cleaning methods, or by heating to melt the deposit.

### **Theoretical Formulation :**

Consider a long pipeline carrying a “waxy” mixture that is completely immersed in water at a constant temperature ( $T_c$ ). This is similar to the transportation of waxy crude oils through sub-sea pipelines from offshore wells. Heat transfer to the surrounding “colder” seawater would decrease the crude-oil temperature ( $T_h$ ), which could lead to the precipitation and deposition of paraffin solids on the pipe wall. As mentioned above, wax crystals would form a deposit layer comprising a solid (wax) phase with immobile liquid oil trapped within it. With time, the deposit layer would grow in thickness until such time that its growth does not occur any more. At this point, the rates of heat transfer across the flowing oil, the wax deposit layer, and the pipe wall would be the same and remain constant with time. When this happens, the thickness of the deposit as well as the oil and wall temperature would each attain a constant value. Once the deposit layer achieves a constant layer thickness, the rate of heat transfer can be assumed to be under a thermal steady state because of the stable temperatures.

As shown schematically with radial temperature profiles in **Fig .1**, the transfer of thermal energy from the “hot” fluid (the flowing crude oil) to the “cold” fluid (the surrounding seawater) at steady state involves four thermal resistances in series: two convective resistances due to the flowing crude oil and the seawater and two conductive resistances offered by the pipe wall and the deposited layer.

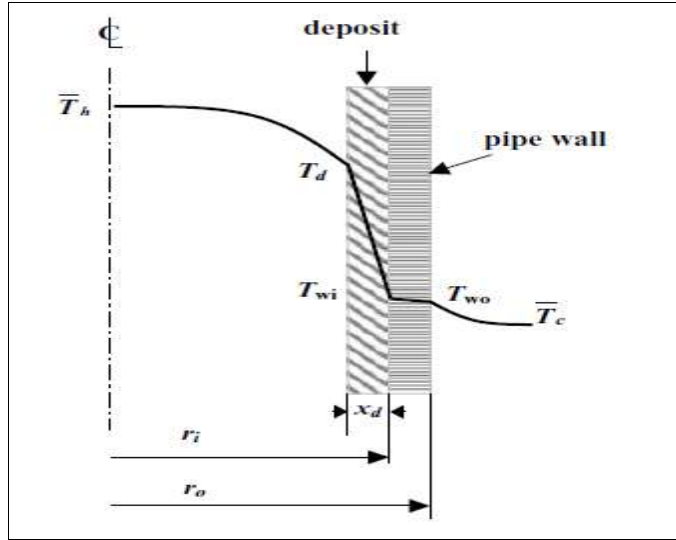


**Figure 1. radial temperature profiles through the various thermal resistances.**

Assuming one-dimensional heat transfer in the radial direction of the pipe, the rate of heat transfer could be equated to the rate of thermal energy lost by the hot waxy crude oil, the rate of thermal energy gained by the cold seawater, and the rate of heat exchange between hot and cold fluids, as follows:

$$q = \dot{m}_h C_h (T_{h \text{ in}} - T_{h \text{ out}}) = \dot{m}_c C_c (T_{c \text{ out}} - T_{c \text{ in}}) = U_i A_i (\bar{T}_h - \bar{T}_c) \quad (1)$$

**Where:**  $q$  = rate of heat transfer.

$\dot{m}_h, \dot{m}_c$  = mass flow rates of “hot” and “cold” streams.

$C_h, C_c$  = average specific-heat capacities of “hot” and “cold” streams.  $T_{h \text{ in}}, T_{h \text{ out}}$  = inlet and outlet “hot” stream temperatures.

$T_{c \text{ in}}, T_{c \text{ out}}$  = outlet and inlet “cold” stream temperatures.

$U_i$  = overall heat-transfer coefficient based on inside pipe surface area ( $A_i$ ).

$\bar{T}_h, \bar{T}_c$  = average temperatures of “hot” and “cold” streams, respectively.

The rate of heat transfer can also be equated to the heat flow across the two convective thermal resistances, as follows:

$$q = h_c A_c (T_{wo} - \bar{T}_c) = h_h A_h (\bar{T}_h - T_d) \quad (2)$$

**Where:**  $h_c, h_h$  = convective heat-transfer coefficients on outside and inside of the pipe, respectively .

$A_c$  = pipe outside surface area in contact with cold stream.

$A_h$  = inside surface area at deposit-oil interface.

$T_d$  = temperature at this interface.

Note that, for a clean pipe with no deposit,  $A_h$  would be replaced by ( $A_i$ ) and ( $T_d$ ) would become equal to ( $T_{wi}$ ).

Next, the overall or combined thermal resistance is expressed as the sum of four individual thermal resistances:

$$\frac{1}{U_i A_i} = \frac{1}{h_h A_h} + \frac{\ln\left(\frac{r_o}{r_i}\right)}{2\pi k_m L} + \frac{\ln\left(\frac{r_i}{(r_i-x_d)}\right)}{2\pi k_d L} + \frac{1}{h_c A_c} \quad (3)$$

At steady state, the heat flux (i.e., the rate of heat transfer per unit inside pipe wall area) through each of the four thermal resistances included in  $U_i$  is as follows:

$$\frac{q}{A_i} = \frac{h_h (\bar{T}_h - T_d)}{\frac{r_i}{(r_i-x_d)}} = \frac{k_d (T_d - T_{wi})}{r_i \ln\left(\frac{r_i}{(r_i-x_d)}\right)} = \frac{k_m (T_{wi} - T_{wo})}{r_i \ln\left(\frac{r_o}{r_i}\right)} = \frac{h_c (T_{wo} - \bar{T}_c)}{\frac{r_i}{r_o}} \quad (4)$$

**Where**  $x_d$  = deposit thickness (assumed to be uniform along pipe length).

$T_{wi}, T_{wo}$  = average inside and outside pipe wall temperatures.

$k_d, k_m$  = thermal conductivities of deposit layer and pipe wall, respectively.

When dealing with the solidification or melting of a pure substance, the liquid-deposit interface temperature ( $T_d$ ) would be the melting or freezing temperature; however, it would be the liquids or saturation temperature for a multicomponent mixture. From a modeling study, Singh et al. [1] estimated ( $T_d$ ) to approach the (WAT) of waxy mixtures when the deposit layer thickness stops growing, while Bidmus and Mehrotra [2] verified experimentally that ( $T_d$ ) and WAT are the same temperature at pseudo-steady-state conditions. The mathematical relationships for heat transfer and energy balance presented above can be utilized for calculations dealing with solids deposition in a pipeline.

#### **Determination of Deposit Thickness( $x_d$ ) at different Crude-oil flow rate:**

“waxy” crude oil is produced and transported via a pipeline from an offshore oil production platform to an onshore refinery for processing. The crude oil has a (WAT) of 26°C. At the beginning of the operation, about 100000, 150000 and 200000 barrels of oil per day (bopd) at a temperature of 40°C leaves the offshore platform into the pipeline. After a few months of pipeline operation, it is observed that the pressure drop across the pipeline has increased considerably and that the crude oil arrives at the refinery at a temperature of 28°C, which has been found to be more or less constant for several days. The engineer managing the operation believes that the increased pressure drop is a result of solids deposition, and the deposit thickness needs to be estimated before deciding on a suitable remedial action. It can be assumed that the seawater at an average temperature of 10°C flows across (or normal to) the pipeline at an average velocity of 0.1 m/s. How could the deposit thickness be estimated from heat-transfer considerations Pertinent pipeline data as well as average crude-oil and seawater properties are listed in **Table 1**.

**Table 1 Data and Average Properties Used in Calculations.**

Property	Value
<b>Crude oil:</b>	
Flow rate(F)	100000, 200000 and 300000 bopd
Specific-heat capacity( $C_h$ )	2400 J/kg K
Thermal conductivity( $k_h$ )	0.15 W/m K
Viscosity( $\mu_h$ )	0.0514082 pa s
Density ( $\rho_h$ )	898.4 kg/m <sup>3</sup>
<b>Seawater:</b>	
Specific-heat capacity ( $C_c$ )	4200 J/kg K
Thermal conductivity ( $k_c$ )	0.65 W/m K
Viscosity( $\mu_c$ )	0.001 pa s
Density( $\rho_c$ )	1020 kg/m <sup>3</sup>
<b>Deposit:</b>	
Thermal conductivity( $k_d$ )	0.24 W/m K
<b>Pipeline:</b>	
Wall thermal conductivity ( $k_m$ )	24 W/m K
Inside diameter ( $D_i$ )	0.254 m
Wall thickness ( $r_o - r_i$ )	0.0159 m
Outside diameter ( $D_o$ )	0.286 m

**Estimation of inside heat-transfer coefficient ( $h_h$ )** : The average velocity of crude oil in the pipeline is:

$$\bar{u}_h = \frac{F}{A_i} = \frac{4F}{\pi D_i^2}$$

The Reynolds number of crude oil in the pipeline is:

$$R_e = \frac{\rho_h \bar{u}_h D_i}{\mu_h}$$



The Prandtl number is:

$$Pr = \frac{C_h \mu_h}{k_h}$$

Given that the flow is turbulent ( $Re > 4000$ ) and assuming  $L/D_i$  to be large, the Holman correlation [3] can be used to estimate the average heat-transfer coefficient in the pipeline ( $h_h$ ):

$$Nu = \frac{h_h D_i}{k_h} = 0.023 Re^{0.8} Pr^{0.3}$$

**Estimation of outside heat-transfer coefficient ( $h_c$ ):**

$$Re = \frac{\rho_c \bar{u}_c D_o}{\mu_c}$$

$$Pr = \frac{C_c \mu_c}{k_c}$$

The Churchill-Bernstein equation [4] can be used to obtain the average heat-transfer coefficient for cross flow across a cylindrical surface:

$$Nu = \frac{h_c D_o}{k_c} = 0.3 + \frac{0.62 Re^{1/2} Pr^{1/3}}{\left[1 + (0.4/Pr)^{2/3}\right]^{1/4}} \left[1 + \left(\frac{Re}{282000}\right)^{5/8}\right]^{4/5}$$

**Estimation of deposit thickness ( $x_d$ ):**

The average oil temperature is  $(T_h) = (40 + 28)/2 = 34^\circ\text{C}$ . As already explained, the deposit-oil interface temperature ( $T_d$ ) will be assumed to be equal to the (WAT) of  $26^\circ\text{C}$ . Therefore, using Eq. (4), we obtain:

$$\frac{h_h(\bar{T}_h - T_d)}{\frac{r_i}{(r_i - x_d)}} = \frac{k_d(T_d - T_{wi})}{r_i \ln\left(\frac{r_i}{(r_i - x_d)}\right)} = \frac{k_m(T_{wi} - T_{wo})}{r_i \ln\left(\frac{r_o}{r_i}\right)} = \frac{h_c(T_{wo} - \bar{T}_c)}{\frac{r_i}{r_o}}$$

Solving these equalities simultaneously for ( $T_{wi}$ ),  $T_{wo}$ , and ( $x_d$ ).

**The Case of Insulated Pipeline:**

With an additional thermal resistance (due to insulation), Eq. (4) becomes:

$$\frac{h_h(\bar{T}_h - T_d)}{\frac{r_i}{(r_i - x_d)}} = \frac{k_d(T_d - T_{wi})}{r_i \ln\left(\frac{r_i}{(r_i - x_d)}\right)} = \frac{k_m(T_{wi} - T_{wo})}{r_i \ln\left(\frac{r_o}{r_i}\right)} = \frac{h_c(T_{ins} - \bar{T}_c)}{\frac{r_i}{(r_i + x_{ins})}} = \frac{k_{ins}(T_{wo} - T_{ins})}{r_i \ln\left(\frac{r_o + x_{ins}}{r_o}\right)} \quad (5)$$

where ( $k_{ins}$ ) and ( $x_{ins}$ ) are the thermal conductivity and the thickness of the insulation material, respectively, and  $T_{ins}$  is the temperature of the insulation material surface in contact with the seawater. Without any solids deposition (i.e.,  $x_d = 0$ ),  $T_{wi} \geq T_d$ . Equation (5), Azevedo, Teixeira[5], therefore, becomes:

$$h_h(\bar{T}_h - T_{wi}) = \frac{k_m(T_{wi} - T_{wo})}{r_i \ln\left(\frac{r_o}{r_i}\right)} = \frac{h_c(T_{ins} - \bar{T}_c)}{\frac{r_i}{(r_i + x_{ins})}} = \frac{k_{ins}(T_{wo} - T_{ins})}{r_i \ln\left(\frac{r_o + x_{ins}}{r_o}\right)}$$

#### Effect of Crude-Oil Composition (WAT):

A change in the crude-oil composition will affect its (WAT). Basically, the waxier a crude oil is, the higher is its (WAT). The effect of wax composition will, therefore, be investigated by varying the (WAT).

Since crude-oil properties and other data (listed in Table1) as well as operating conditions are the same, the individual heat-transfer coefficients can be used. Equation (4) can be solved for ( $x_d$ ) by substituting the given (WAT) values for the interface temperature ( $T_d$ ).

#### Effect of Crude-Oil and Seawater Temperatures:

Using Eq. (4) with the same properties and heat-transfer coefficients, we get ( $x_d$ ).

#### Results:

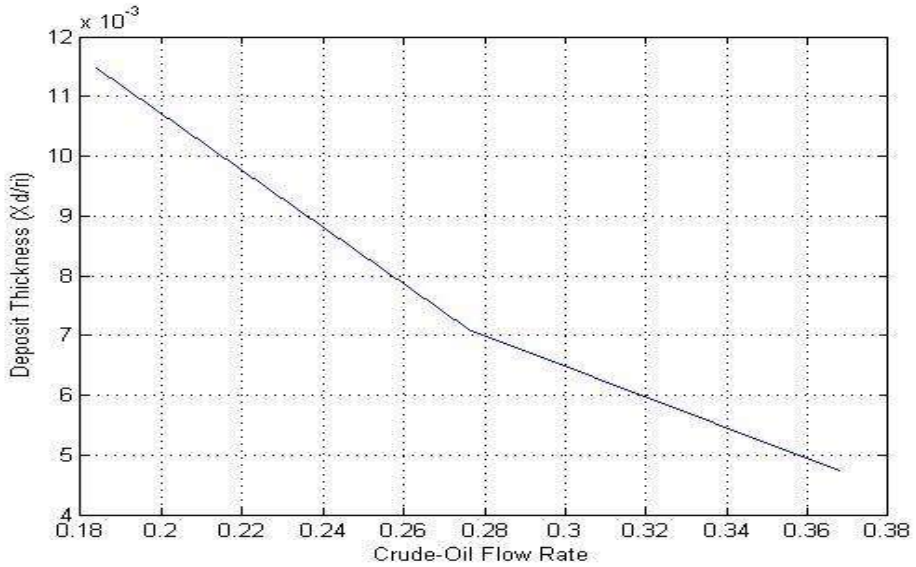


**Figure 2. Effect of Crude-Oil Flow Rate on deposit thickness under similar operating conditions at 0.184 m<sup>3</sup>/s.**

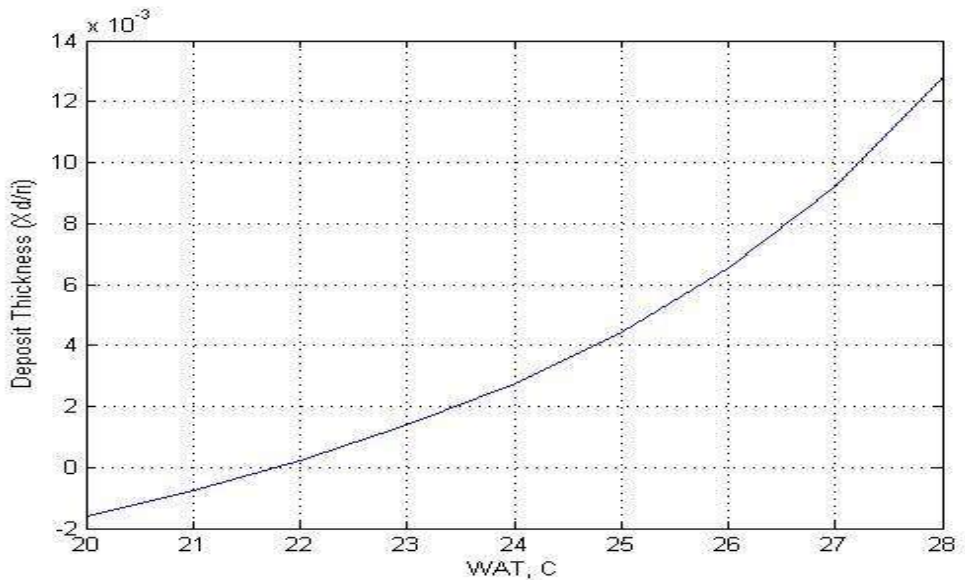


**Figure 3. Effect of crude-oil WAT on deposit thickness under similar operating conditions at 0.184 m<sup>3</sup>/s.**

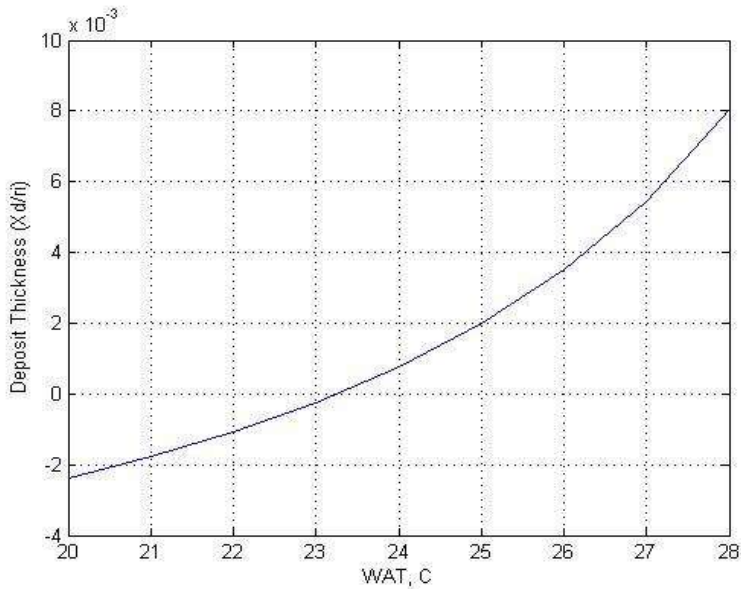


**Figure 4. Effect of crude-oil WAT on deposit thickness under similar operating conditions at 0.276 m<sup>3</sup>/s.**

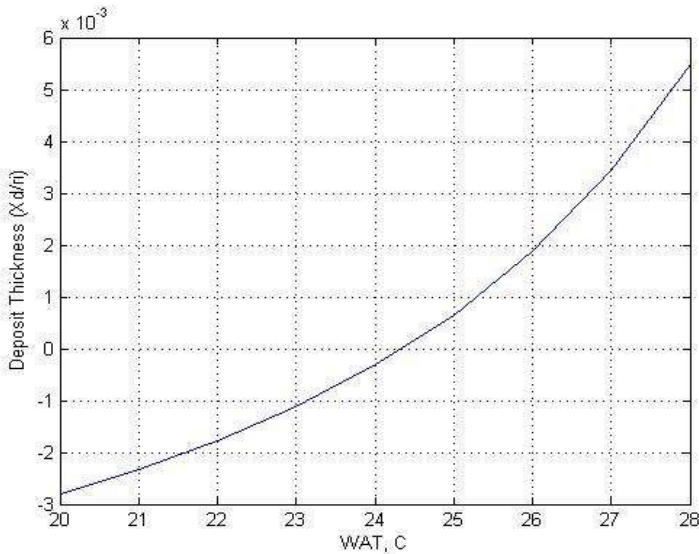


**Figure 5. Effect of crude-oil WAT on deposit thickness under similar operating conditions at 0.368 m<sup>3</sup>/s.**

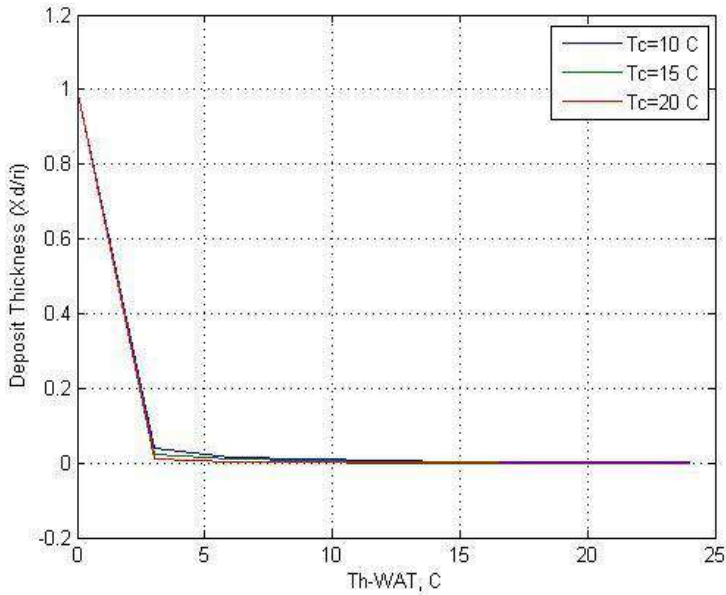


**Figure 6. Predicted variations in deposit thickness with crude-oil temperature at different seawater temperatures at 0.184 m<sup>3</sup>/s.**

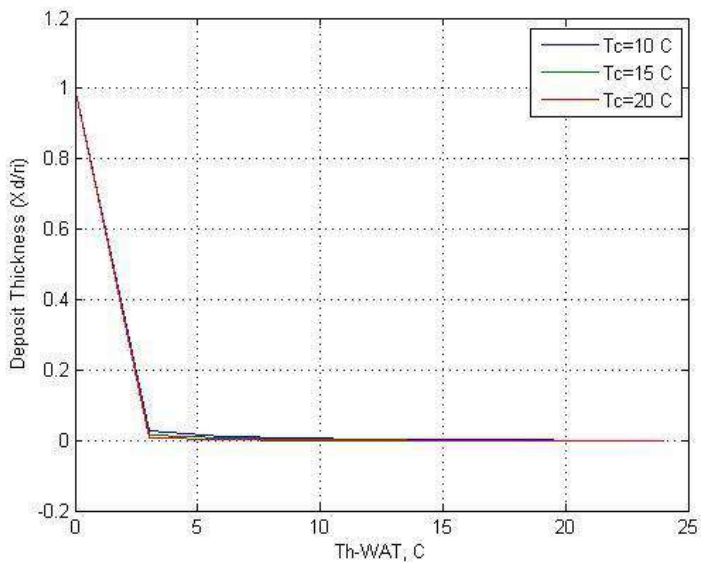


**Figure 7. Predicted variations in deposit thickness with crude-oil temperature at different seawater temperatures at 0.276 m<sup>3</sup>/s.**

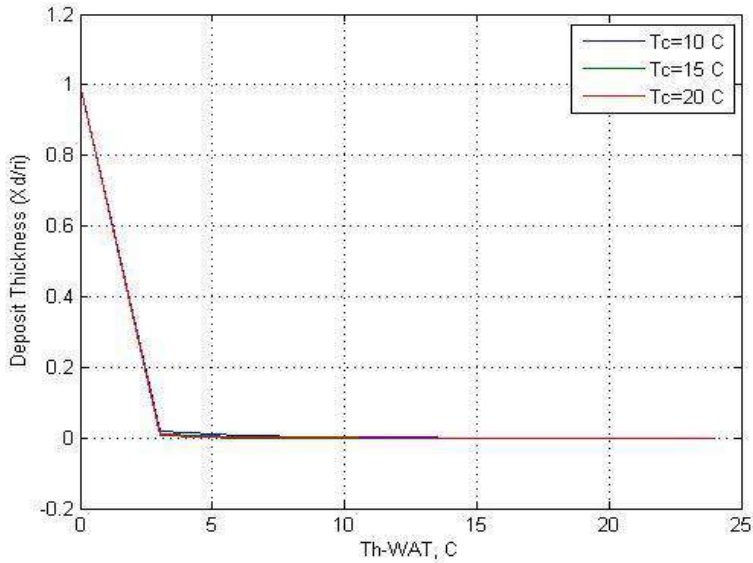


**Figure 8.** Predicted variations in deposit thickness with crude-oil temperature at different seawater temperatures at  $0.368 \text{ m}^3/\text{s}$ .

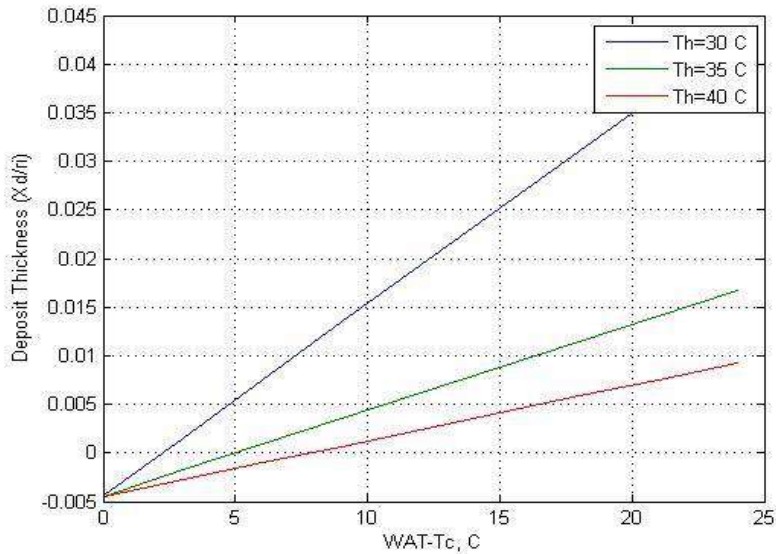


**Figure 9.** Predicted variations in deposit thickness with seawater temperature at different crude-oil temperatures at  $0.184 \text{ m}^3/\text{s}$ .

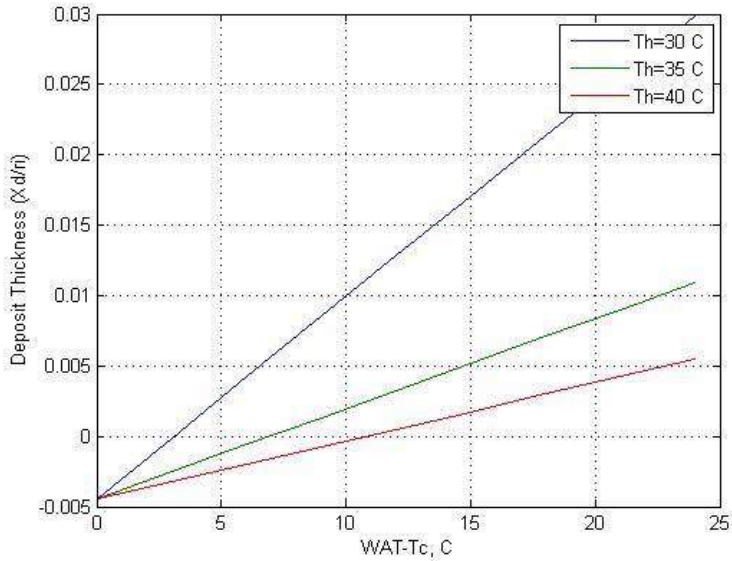


**Figure 10. Predicted variations in deposit thickness with seawater temperature at different crude-oil temperatures at  $0.276 \text{ m}^3/\text{s}$ .**

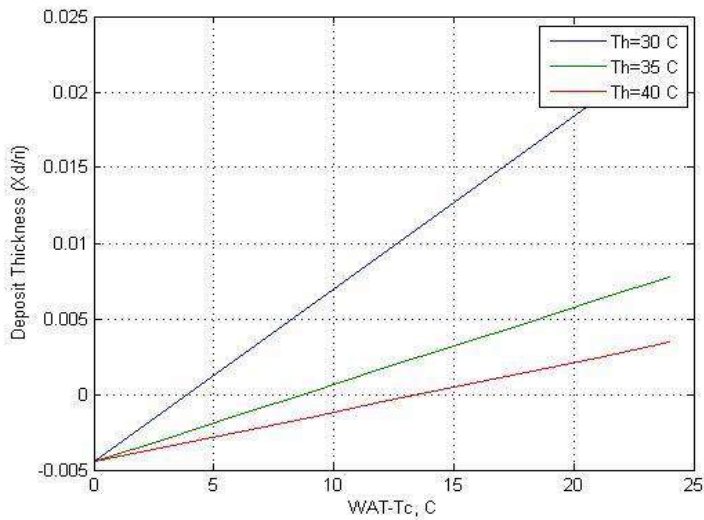


**Figure 11. Predicted variations in deposit thickness with seawater temperature at different crude-oil temperatures at  $0.368 \text{ m}^3/\text{s}$ .**

## Conclusion:

- The deposit thickness is reduced as a result of an increase in the crude-oil flow rate. This is caused by the increased inside heat-transfer coefficient due to the increased flow rate. The resulting higher wall temperature then yields a reduction in the amount of deposition.
- The predictions are shown in **Figs.3** and **4**, which indicate that there is a reduction in the amount of deposited solids with an increase in either the crude-oil temperature or the seawater temperature. Conversely, a reduction in either the crude-oil or the seawater temperature would yield a larger amount of deposited solids. These predictions are in good agreement with experimental results reported by Mehrotra and Bidmus [6], who had performed wax deposition experiments over a range of operating conditions using a concentric draft tube assembly with a “hot” wax-solvent mixture flowing in the inner tube and cold water flowing through the annular region.
- The higher WAT gave a larger deposit thickness and a lower WAT of gave a smaller deposit thickness of. These results imply that an increase in the crude-oil wax concentration would lead to an increase in the amount of deposit in the pipeline. This effect is further illustrated in **Fig.2**, where the deposit thickness has been obtained for WAT values ranging from 20 to 27°C. It should be noted that, in these calculations, it was assumed that all crude-oil properties remain constant even though the concentration of wax was varied. Properties such as the viscosity and density of the crude oil can be altered by an increase in wax concentration, which would alter the value of inside heat-transfer coefficient. However, even with such crude-oil property changes, an increase in wax concentration would lead to increased amount of deposit in the pipeline.
- During the solids deposition process, the deposit layer acts as an insulation to heat transfer, thereby preventing further solids deposition. The importance of the deposit thermal conductivity is illustrated in case study. Also note the much larger temperature difference across the insulation material.



## References:

- [1]Singh, P., Venkatesan, R., Fogler, H. S., and Nagarajan, N., “Formation and Aging of Incipient Thin Film Wax-Oil Gels,” *AIChE J.* 46, 1059, 2000.
- [2]Bidmus, H. O., and Mehrotra, A. K., “Heat-Transfer Analogy for Wax Deposition from Paraffinic Mixtures,” *Ind. Eng. Chem. Res.* 43, 791, 2004.
- [3]Holman, J. P., *Heat Transfer*, 9th ed., McGraw-Hill, New York, 2002.
- [4]Churchill, S. W., and Bernstein, M. A., “Correlating Equation for Forced Convection from Gases and Liquids to a Circular Cylinder in Crossflow,” *J. Heat Transfer* 99, 300, 1977.
- [5]Azevedo ,L.F.,Teixeira,A.,A critical review of the modeling of wax deposition mechanisms, *Potroleum Science and Technology*, Vol21,No3,ed4 393-408,2003.
- [6]A.Mehrotra,H,Bidmas, Heat transfer calculation for predicting solid deposition in pipelines transportation of waxy cruds. Dept. of chemical Eng. univ. of Calgary Canada.

## Estimation of cementation factor for a field of around Brack sandstone Reservoir

Khaled taleb<sup>1</sup>, Hakim Shebbani<sup>2</sup>, Abduraof. A.Al amari.<sup>3</sup>

1,3 .Faculty of Engineering ,Gharyan University

.2 Higher Institute of Science and Technology, Gharyan.

### المخلص:

يعتبر إيجاد معامل التماسك هو العامل الأكثر أهمية خلال دراسة تشبع الهيدروكربون/الماء من قياسات المقاومة الكهربائية على اللباب السدادى أو من سجلات خط الاسلاك باستخدام معادلة أرشي. ومن تم تحديد قيمة عامل التثبيت بدقة. الهدف من هذه الدراسة البتروفيزيائية هو الحصول على عامل تدعيم أكثر واقعية لبعض عينات من مكنم الحجر الرملي. تم إنشاء المخططات التبادلية بين عامل مقاومة التكوين والمسامية لنقاط البيانات المقاسة ، ومن تم الحصول على قيم عامل الهندسة الداخلية  $a$  وعامل التماسك  $m$  من المخططات المتقاطعة لكل حقل. أظهرت المخططات المتقاطعة علاقة جيدة بين الخاصيتين  $F$  ,  $\phi$  حيث تم حساب الخطأ القياسي لنقاط البيانات الفعلية للحقل ، ويرجع ذلك أساسا إلى عدم التجانس الداخلي والمزيد من الكسور في تكوين الحجر الرملي للحقل. كما تم حساب النسبة المئوية المتوسطة للأخطاء النسبية بين المعادلة الأساسية ( **Humble Equation** ) ونقاط البيانات الفعلية والارتباط أو العلاقة الجديدة ونقاط البيانات الفعلية للحقل.

### ABSTRACT:

Estimation of cementation factor is one of the most important factors in determining the hydrocarbon/water saturations. In order to determine this factor accurately, core sample porosity, formation water resistivity and resistivity of the core sample hundred percent saturated by formation water, were performed using the Archie equation. The objective of this petro physical study is to obtain a more realistic cementation factor for some sandstone reservoir core samples. cross-plots between formation resistivity factor and porosity were created for measured data points The values of internal geometry factor  $a$  and cementation factor  $m$  were obtained from the cross -plots for each field .the cross-plots showed a good relationship

between the two properties  $F$  &  $\emptyset$  where the standard error for the actual data points was calculated for a field. This is mainly due to the internal heterogeneity and more fractures in the Brack sandstone formation of field-Q. Also the percentage average relative errors between the humble equation and the actual data points and the new correlation and the actual data points were calculated for this field.

**Keywords: cementation factor, porosity, formation resistivity factor, rock samples.**

## INTRODUCTION:

Petrophysical science is the science concerned with studying the physical properties of rocks and their relationship with fluids. Successful assessments of petrophysical reservoir properties are essential to determine the hydrocarbon capacity and reservoir system action, and help researchers predict the behavior of complex reservoir settings[1]. Previous research indicated that cementation factor value is greatly influenced by porosity, porous throat volume, water and mineral conductivity, and surface area per unit volume and cement. The cementation factor usually depends on the shape and surface area of the compound particles and the tortuosity factor [2-3]. The cementation factor in study was determined by using the experimental data. These measured data including core sample porosity, formation water resistivity and resistivity of the core sample hundred percent saturated by formation water. The analysis of these data were showed that more accurate value for cementation factor can be derived. the data were used in this study are from several wells in field. The Brack formation of the eastern sirte basin consists of mainly sandstones and shale's resting with non-conformity on a basement complex of igneous and metamorphic rocks, and overlain by the upper cretaceous clastic rocks. The Brack formation is subdivided into three layers. the Brack sandstone represent braided and meandering fluvial deposit, where as the middle member Nubian represents shallow lake deposit. The layers of Brack formation comprise mainly of sandstone interbedded with siltstones and shale's. the Middle Nubian consists of shale's and silty shales.

## Porosity:

Porosity is one of the most important petrophysical properties, which is a measure of the storage capacity of hydrocarbon. Porosity is defined as the

ratio of the pore space within the rock to the total volume of the rock .porosity is created as a result of imperfect contact between rock grains .the void space created between the rock grains is called pore volume and the remaining part of the rock that occupied by the rock grains is called grain volume. Therefore, porosity can be expressed mathematically as

$$\phi = V_p/V_b \quad , \quad \phi = V_p/(V_p+V_g) \quad (1)$$

$\phi$  Fractional porosity

$V_p$  pore volume

$V_g$  Grain volume

$V_b$  Bulk volume

The porosity of petroleum reservoir ranges from 5% to 40%, which depends on rock texture and the diagenetic process. Porosity is independent of grain diameter but strongly depends on packing and sorting in general small grain size and high angularity tends to increase porosity while an increase in particle size range (sorting) tends to decrease porosity [4].

### Resistivity:

Electric resistivity was the earliest and still the most frequently measured physical property of rocks to locate oil and gas reservoirs [5]. Electrical resistivity methods involve the measurement of the apparent resistivity of soils and rock as a function of depth or position. The electrical resistivity of a material is its ability to resist or impede the flow of electric current. The resistivity of rocks is a complicated function of porosity, permeability, ionic content of pore water, and clay mineralization. Dry rocks are poor conductors; therefore, they normally exhibit extremely high resistivity [6]. Reservoir rocks are porous and their pores are generally saturated with water, oil and gas .the formation water normally has resistivity of 0.04 to 10 ohm.m at 70°F, which is much lower than that of the rock grains .As a result, they are conductors of moderate conductivity when they are saturated with water. The electric resistivity of a material can be defined by the following equation

$$R = r * A/L \quad (2)$$

**Where:**

R Resistivity

r Resistance

A cross-sectional area of the conductor available to current flow

L Length of the conductor

A/L Geometric factor which, which depends on the geometrical shape of the investigated rock Porosity and resistivity relationship (the concept of formation resistivity factor)

Archie (1942) found that the resistivity 100 % water saturated rocks is directly proportional to the resistivity of the water that saturates them [7]. The constant of proportionality is called formation resistivity factor (FF), which is defined as the ratio of the resistivity of the fully saturated rock to the resistivity of the water that saturates its pore space .

$$FF = R_o / R_w \quad (3)$$

A strong dependence of formation resistivity factor on porosity was observed Archie (1942). A large number of measurements on rock samples showed that the formation resistivity factor of shale – free rocks could be related to porosity by:

$$FF = \phi^{-m} \quad (4)$$

Where FF is the formation resistivity factor,  $\phi$  is the fractional porosity and m is cementation exponent. The above equation implies that a graphical presentation, the logarithm of the formation resistivity factor FF versus the logarithm of the fractional porosity  $\phi$  is a straight line with slope m [8]. Thus, cementation factor m as a function of formation resistivity factor FF and porosity  $\phi$  is

$$m = -\log FF / \log \phi \quad (5)$$

Therefore, m is generally referred to as the cementation factor; archie relationship was later modified by winsaure to the general form .

$$F = a / \phi^m \quad (6)$$

Where a was defined as a constant and is a function of the tortuosity of the capillary path in the rock. winsaure, et al applied the general Archie form in

sandstone formation and they obtained  $m = 2.15$  and  $a = 0.62$ . This equation is known as the Humble equation and it is the most widely used for sandstone in the world [9].

$$F = 0.62 / \phi^{2.15} \quad (7)$$

The most widely used form of Archie equation for both limestone and dolomites is basic: [10-11]

$$F = 1 / \phi^2 \quad (8)$$

### Experimental Technique:

Full diameter cores from six wells from Brack sandstone were prepared cleaned dried and left to cool in room temperature before conventional core analysis commenced. The cell helium expansion gas porosimeter used for measurement the grain volume of samples and calculate the porosity and bulk volume by early equations. The Formation resistivity factor was measured for the previous samples. The clean, dry samples were loaded in a stainless steel saturator and evacuated for 12 hours. A solution of 170 g /l (for x1-x6) sodium chloride was introduced at the end of the period, followed by pressurizing the system at 2000 psig for 12 hours to assist penetration.

The bring saturated plugs were placed in turn between electrodes at 1KH frequency and their electrical resistances were measured consecutive days until ionic equilibrium was achieved between the fluid and rock samples

Formation factor measurements are made on 100% brine saturated rock sample either at ambient conditions or elevated reservoir overburden pressure. Sample resistance is measured and converted to resistivity using sample cross-sectional area and length. Formation resistivity factor is calculated as the ratio of the sample resistivity to the resistivity of the water saturating it. The formation resistivity factor of a group of samples is plotted versus their porosities on log-log graph paper. The slope of the best fit line is the value of the cementation factor,  $m$  and the intercept is the value of,  $a$ .

### Data Analysis procedures :

\*The formation resistivity factor (F). was calculated for each well using Archie equation:

$$F = R_o / R_w$$

\*The formation resistivity factor (F) was plotted against the porosity ( $\emptyset$ ) on logarithmic scales for each well and for each field[12].

\*Calculated **m** , **a** from the logarithmic cross plot and the standard error was determined.

Where:

**a** = represent the intercept of an extrapolated trend line on logarithmic F &  $\emptyset$  cross – plot with the porosity axis equal one.

**m** = represents the slope of trend line..

Standard error is the positive and negative error of the actual data points.

For each constant **a** & **m** the formation resistivity factor was calculated using the general form of Archie equation

$$F = a / \emptyset^m$$

\*The relative error between the actual equation and Humble equation was calculated.

$$FA = R_o / R_w \quad \text{Actual Equation}$$

$$FH = 0.62 / \emptyset^{2.15} \quad \text{Humble Equation}$$

$$\text{Relative \%} = ((FH - FA) / FA) * 100$$

\*calculate the average error between the actual equation and Humble equation using the following equation:

$$\text{Average error \%} = \text{Sum error \%} / \text{no. of point}$$

\*Calculate the relative error between the actual equation and the new correlation.

$$FA = R_o / R_w \quad \text{Actual Equation}$$

$$FN = a / \emptyset^m \quad \text{New correlation}$$

$$\text{Relative error \%} = ((FN - FA) / FA) * 100$$

\*Calculated the average error between the actual equation and new equation.

$$\text{Average error \%} = \frac{\text{Sum error \%}}{\text{no. of point}}$$

The cross-plots of the formation resistivity factor versus porosity for wells Q2,Q4,Q5 and Q6 are showing blew, the cross-plots illustrate the obtained internal geometry factor **a** , cementation factor **m** ,correfficient **R<sup>2</sup>** and the stander error.

**Table (1) shows the measured data of well Q2**

Well #	Sample #	Porosity fraction	R <sub>w</sub> ohm-m	R <sub>o</sub> ohm-m	FA
Q2	1	0.1021	0.061	5.290	86.72
	2	0.1571	0.061	1.886	30.92
	3	0.0709	0.061	4.610	75.57
	4	0.0964	0.061	3.613	59.23
	5	0.0802	0.061	5.185	85.00

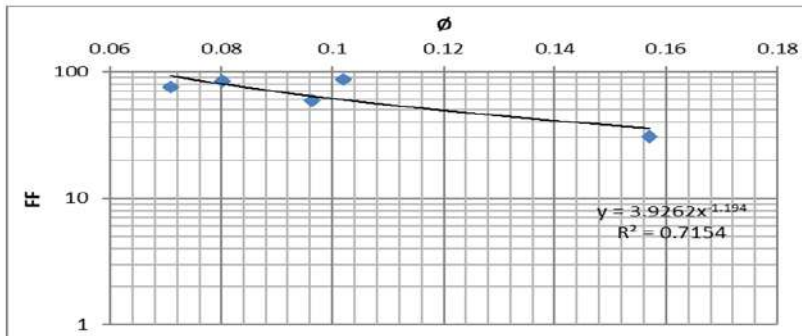


**Figure (1) shows the formation resistivity factor versus porosity fro well Q2**



**Table (2) shows the measured data of well Q4**

Well #	Sample #	Porosity fraction	Rw ohm-m	Ro ohm-m	FA
Q4	1	0.062	0.061	4.469	73.26
	2	0.131	0.061	2.365	38.77
	3	0.0992	0.061	3.068	50.30
	4	0.0879	0.061	3.135	51.39
	5	0.1443	0.061	1.804	29.57
	6	0.0545	0.061	4.574	74.98
	7	0.0961	0.061	3.384	54.89
	8	0.074	0.061	4.362	71.51
	9	0.1053	0.061	2.130	34.92
	10	0.0639	0.061	4.256	69.77
	11	0.1696	0.061	1.555	25.49

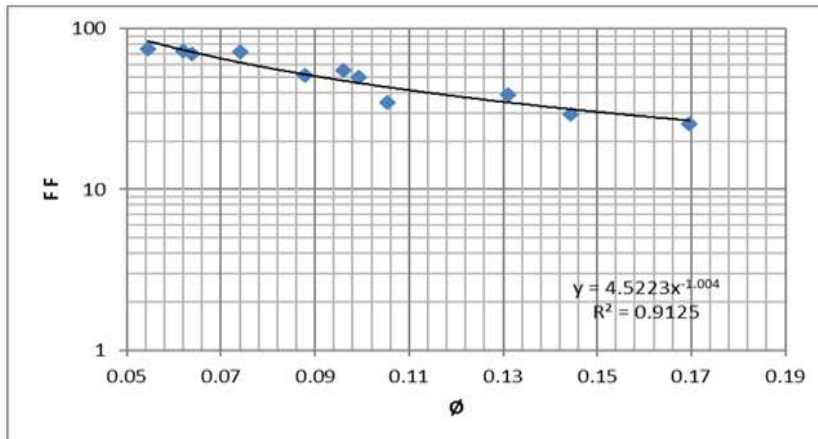


**Figure (2) shows the formation resistivity factor versus porosity from well Q4**

**Table (3) shows the measured data of well Q5**

Well #	Sample #	Porosity fraction	Rw ohm-m	Ro ohm-m	FA
Q5	1	0.1731	0.061	1.995	32.70
	2	0.1037	0.061	2.968	48.66
	3	0.1271	0.061	2.372	38.15
	4	0.1372	0.061	2.072	33.97
	5	0.1418	0.061	2.901	47.56
	6	0.1262	0.061	2.332	38.23
	7	0.1201	0.061	3.357	55.03
	8	0.1218	0.061	1.695	27.79
	9	0.1366	0.061	2.221	36.41
	10	0.1049	0.061	3.507	57.49
	11	0.1022	0.061	3.361	55.10
	12	0.1301	0.061	2.102	34.46
	13	0.1054	0.061	3.179	52.11
	14	0.1473	0.061	1.671	27.39
	15	0.1617	0.061	1.548	25.38
	16	0.0963	0.061	3.430	56.23

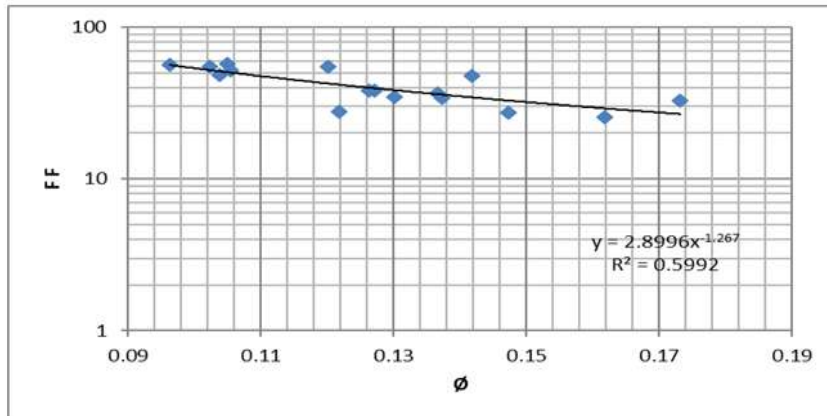


**Figure (3) shows the formation resistivity factor versus porosity from well Q5.**

**Table (4) shows the measured data of well Q6**

Well #	Sample #	Porosity fraction	Rw ohm-m	Ro ohm-m	FA
Q6	1	0.132	0.061	2.489	40.80
	2	0.1016	0.061	4.338	71.11
	3	0.0936	0.061	4.871	79.85

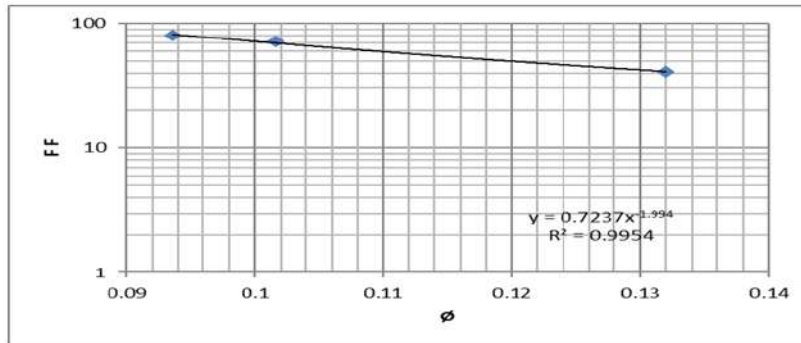


**Figure (4) shows the formation resistivity factor versus porosity from well Q6**

**Table (5) shows the results of internal geometry factor a, cementation factor m and the standard error for all field.**

Well #	Internal geometry factor a	Cementation factor m	Standard error
Q2	3.94	1.19	0.11486
Q4	4.54	1.00	0.04873
Q5	2.90	1.27	0.07970
Q6	0.72	1.99	0.01506
Field	2.96	1.25	0.0776

### Results and discussion:

The cross-plots of formation resistivity factor against the fraction porosity on the logarithmic scale were showed a good correlation all wells in the field .many samples selected from all wells and represent around the sandstone formation were used in this petrophysical analysis .

The following are the results of an average relative error of field.

- The average relative error of field from Humble equation is equal 62.18%.

- The average relative error of field from New correlation is equal 1.36%.

## Conclusions :

- More realistic values for cementation factor  $m$  and the internal geometry factor  $a$  were derived from this petrophysical study for the field representing the Brack sandstone formation and using Archie general equation the proper correlation for field.

$$F = 2.96 / \phi^{1.36}$$

- The calculated error of the data points when deriving the correlation was very small which indicated that the correlation is consistent.
- This study showed that Humble equation could not be applied for this formation due to the large difference and error, which were observed between this equation and the actual data points.
- The study showed using of the experimental data to derive the values of  $a$  &  $m$  will produce more accurate and correct results .

## References:

- [1] Saeed,R ,and Abdlnabi, H. , A New Cementation Factor Correlation in Carbonate Parts of Oil Fields in South – West Iran "Iranian Journal of Oil & Gas Vol.3(2014),No. 2,pp.01-17
- [2] Hilmi .S and Geage. V ,The cementation factor of Archie s equation for shaly sandstone Journal of Petroleum Science and Engineering 23 \_1999. 83–93.
- [3] Fadhil.s.k and Arffin.S. A review correlations between Cementation Factor and Carbonate Rocks Properties "Life Science Journal 2013 ; 10(4)
- [4] Tiab, D. and Donaldson,E.C.,1996,Petrophysics ,ISBN 0-88415-634-6.
- [5] 5 Salem,H.S. Determiation of porosity ,formation resistivity Factor, Archie cementation Factor and Pore geometry for a Glacial aquifer, Energy Sources ,1July 2001, vol.23,n06,pp.589-596.
- [6] Keller G. V., (1989) Electrical properties in CRC Practies Handbook of physical properties of rocks and minerals. Edited by R.S. carmichael.
- [7] Archie,G.E.,1942"The electrical resistivity log as an aid in determining some reservoir characteristics", Trans.AIME, vol.146,pp,54-62
- [8] Masoud.A , Ali.M , , Monouchehr.H , Mehran.N.Invistigation of cementation factor in iranian carbonate reservoirs, The 14th Formation Evaluation Symposium of Jpan, September 29-30 , 2008.

- [9] Dr.bahia.A , Dr Khulud.M. Variety of cementation factor between dolomite and quartzite reservoir. Tripoli university bulletin 2017.
- [10] Walid.M.M, and Khaled.S.S A numerical technique for an accurate determination of formation resistivity factor using FR-RO Overlays method "Arab J Geosic(2015) 8;1291-1297.
- [11] Focke, J. W. and Munn, D., Cementation Exponents in Middle Eastern Carbonate Reservoirs, SPE Formation, June 1987.
- [12] Elias Raul D, Enesto Rosales Z, Tortosiy and cementation factor parameters: A review on their determinations, Rosales Zambrano Ingenieiria (RZI) , 2017.

## Analyzing and Modeling the Separation Distance of Lightning Arresters for 400kv Transfer Substation's Protection against the Lightning Strokes

Imhimmad Abood<sup>1</sup>, Ahmed altawwary<sup>2</sup> and Abdhakeem Alkwas<sup>3</sup>

1- University of Gharian, faculty of engineering , email: aboodali1966@gmail.com

2- High institute for sciences and technology Gharian, electric dept. email: as69287@gmail.com

3 - University of Sabratha, faculty of engineering, email: ash\_hakem@yahoo.com

### المخلص

تتعرض الشبكات القدرة الكهربائية ( ذات الجهد العالي ) إلى ضربات الصواعق أحيانا ( ناتجة عن البرق) ذات جهد عالي عابر عالي القيمة ونتيجة لذلك ترتفع جهود النظام العابرة إلى قيم عالية جدا قد تؤدي إلى دمار أحد مكونات الشبكة الكهربائية ، ولفهم هذه الظواهر و تتمكن من تفادي خطرهما على أنظمة القدرة الكهربائية يجب استعمال برامج متطورة لمحاكاة الشبكات ودراسة تأثير هذه الجهود الزائدة العابرة وطرق الحماية منها لتحسين أداء الشبكة تحت هذه الظروف ، حيث تم اختيار برنامج الموجات الكهرومغناطيسية (ATP) لهذا الدراسة، وكان الهدف من هذا البحث هو تحليل و دراسة تأثير ضربات الصواعق وطرق الحماية منها باستخدام حاجزة الصواعق ( Lightning Arrester ) وكذلك دراسة تأثير بعد حاجزة الصواعق عن المحول لحماية محطة تحويل الجهد العالي (400KV) من ضربات الصواعق، وتم الاختبار على شبكة نقل ومحطة تحويل جهد 400KV مكونة من أربعة أبراج، تتعرض هذه الشبكة إلى ضربات صاعقة بتيارات مختلفة مع تغير بعد الحاجزة عن المحول، وكانت الدراسة مدعومة بنوعين من حاجزات الصواعق (Zinc Oxide-porcelain) و (EXLIM Q1) و (Zinc Oxide-silicone polymerPEXLIM Q2) أظهرت نتائج الدراسة ان تحديد المسافة بين حاجزة الصواعق و الوحدة المراد حمايتها ونوعية حاجزة الصواعق تلعب دورا مهم في توفير الحماية وعدم خروج المحطة عن العمل.

## Abstract

This paper presents a study modification of separation distance of lightning arrester protecting a 400KV sub-station from lightning strokes related to the distance between the transformer and lightning arrester (the installation place of the lightning arrester ) a simple model was created in ATP and the distance between the arrester and transformer were varied. to ensure proper installation and to reduce the high lightning failure rate and to eliminate devastating impact, caused by lightning, the model e installation represents circuit composed of four towers . Program ATP-Draw (Alternative Transient Program) was used to simulate the problem. The simulation was done on three stages and the results were compared.

Key Words : lightning arrester, current, distance (the installation place of the lightning arrester related to protected unit), transformer

## 1.0 -Introduction

Sub-stations are the most sensitive part in power systems and are exposed to many stresses, like Transients over voltages which caused by lightning discharges or switching operations. So Lightning is the main reason for outages in transmission and distribution lines [1].

A surge lightning arrester is a protective device which is must be used in to substations to be protected. The highly non-linear characteristics of an arrester allow the arrester to limit the voltage across its terminal during conduction of surge current, arrester exhibits very low impedance. This study was executed using two kinds of lightning arresters Zinc Oxide PEXLIM –Q2) and (Zinc Oxide EXILIM –Q1). the 1980s polymeric ZnO surge arresters have been developed quickly and put into operation on transmission lines in parallel with the insulators to limit the over voltages based on their excellent performance [2], [3],[4]

## 2.0 - System under study:

This part introduces single line diagrams of the 400kv network. Which has triplet bundle conductors. Tower footing resistance of this system is 10  $\Omega$  and the range of lighting current is 300KA with negative peak and the following fig (2.1) shows model for a 400kV network. The Physical

specifications of conductors and geometrical parameters of the tower are given in table (2.1).

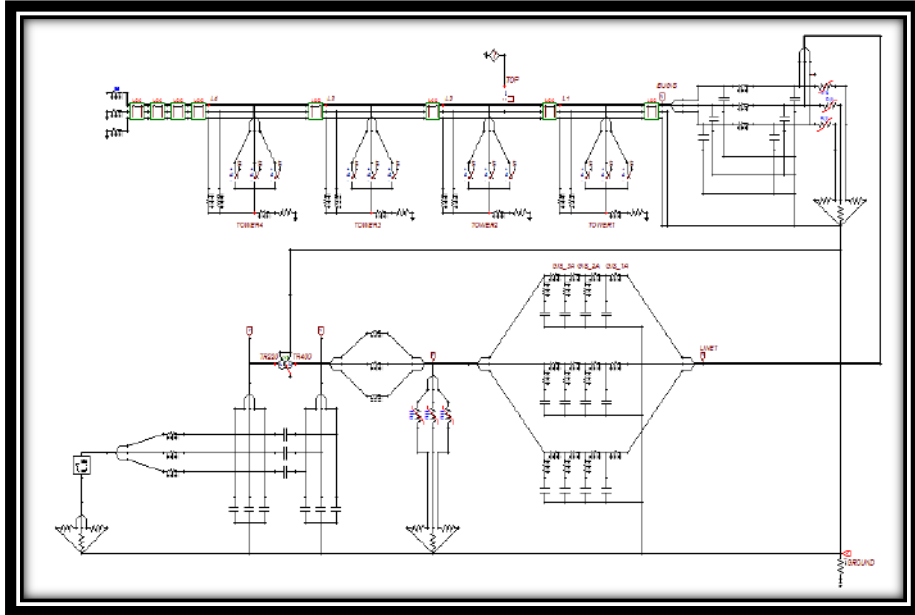


Fig (2.1): Shows the structure of 400kv studied system circuit modeled in ATP

## 2.1 -Conductor characteristics:

Table (2.1): Conductor characteristics:

Ph.no	$R_{in}$	$R_{out}$	$R_{ho}$	$H_{horiz}$	$V_{tower}$	$V_{mid}$	$Separ$	$Alpha$	$N.b$
	(cm)	(cm)	$\Omega/kmDC$	M	M	m	Cm	Deg	
1	0	1.3195	0.079	-11.38	41.7	27.4	40	30	3
2	0	1.3195	0.079	0	42.7	28.4	40	30	3
3	0	1.3195	0.079	11.38	41.7	27.4	40	30	3



## 2.2-Ground wire characteristics:

Table (2.2) shows the vertical and horizontal distances of the conductor and the ground wire from the surface.

**Table (2.2): Ground wire characteristics**

Ph.no	$R_{in}$	$R_{out}$	$R_{ho}$	$H_{oriz}$	$V_{tower}$	$V_{mid}$	Separ	Alpha	N.b
	(cm)	(cm)	$\Omega/\text{kmDC}$	M	M	M	Cm	Deg	
4	0.48	0.87	0.3	-6.28	51.27	39.07	0	0	0
5	0.48	0.87	0.3	6.28	51.27	39.07	0	0	0

**Table (2.3): Conductor arrangement of overhead transmission line**

Number.ph	Vertical	Horizontal
1	41.7 m	-11.38m
2	42.7 m	0
3	41.7 m	11.38m
Ground wire	Vertical	Horizontal
4	51.27 m	0 m
5	51.27 m	0 m

## 3.3 Surge arresters those were used in an electrical circuit

### 3.3.1-First arrester (Zinc Oxide EXILIM-Q1):

Table (3.1) shows brief performance data.

**Table (3.1): Brief performance data**

System voltage	170-420kv
Rated voltage	42 - 360kv
Nominal discharge current	20 KA
Line discharge class	Class 4
Short-circuit	65kA
Mechanical Strength	2500Nm
Design altitude	max 1800m

Ambient temperature	-50 C° to +45 C°
Frequency	15 – 62 Hz

### 3.3.2–Second arrester (Zinc Oxide PEXLIM –Q2)

Table (3.2) shows brief performance data.

**Table (3.2): Brief performance data**

<b>System voltage</b>	<b>52 - 420kv</b>
Rated voltage	42 - 420kv
Nominal discharge current	10 KA
Line discharge class	Class 3
Short-circuit	50kA
Mechanical Strength	2500Nm
Design altitude	max 1800m
Ambient temperature	-50 C° to +45 C°
Frequency	15 – 62 Hz

The surge arrester characteristic of the 400kv network is from General Electrical Company of Libya (GECOL).

#### 4.0 - ATP Analysis of 400kv circuit diagram:

Three cases were done to test the system under study. In each case it will be calculated extent the basic insulation level (BIL) of the transformer and then shows the impact of the lightning on the transformer insulator.

##### 4.1-First Case:

- 1- The ground wire (shielding line) of the overhead transmission lines exposed to lightning stroke. The lightning current of the stroke is fixed (260kA). With changing the separation distance between (the installation place of the lightning arrester ) and the transformer from (5m to 30m), increasing 5m each step using the two types of lightning arresters and

measuring the resulting of the internal voltage on the primary winding of transformer and basic insulation level (**BIL**)of the transformer for both lightning arresters.

**Fig (4.1)** shows the values of the internal voltages of the primary side of transformer the distance 5m lightning current 260kA using (Zinc Oxide EXILIM – Q1).

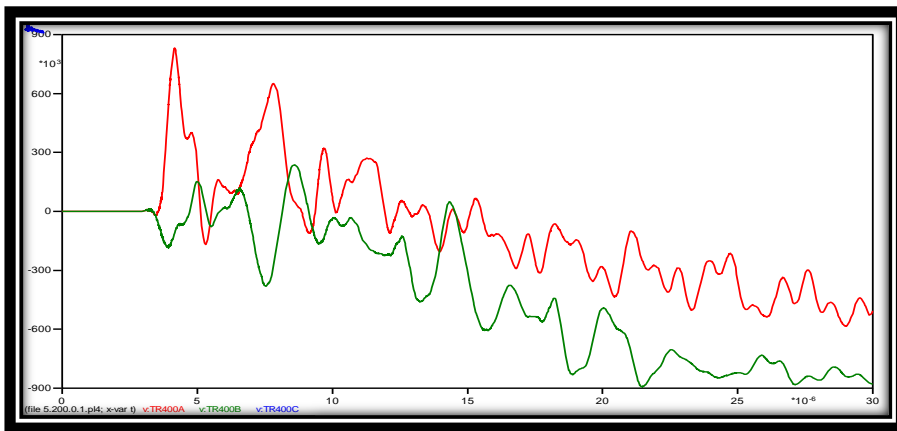


**Fig (4.1):** the transient over voltage on the primary winding of the transformer when distance (5m) and the lightning current (260 KA)

**Fig (4.2)** shows the values of the internal voltages of the transformer the distance 10m and the lightning current is fixed (Zinc Oxide EXILIM – Q1).

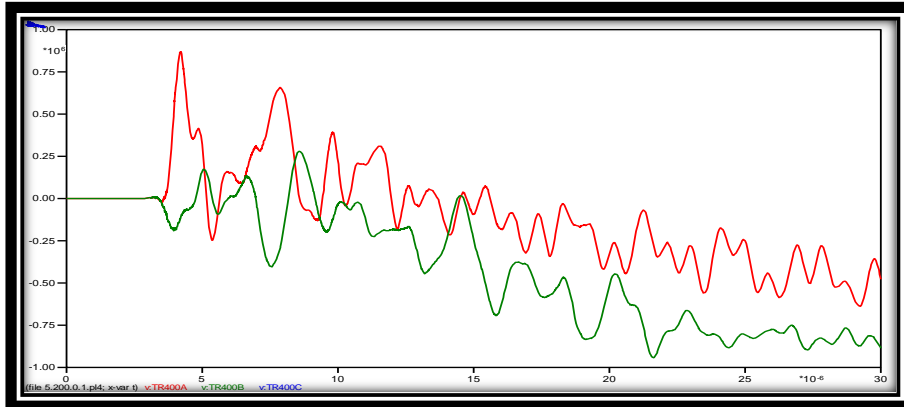


**Fig (4.2):** the transient over voltage on the primary winding of the transformer when distance( 10m) and the lightning current( 260 KA)

**Fig (4.3)** shows the values of the internal voltages of the transformer the distance 5m keeping the current fixed (Zinc Oxide PEXLIM –Q2)..

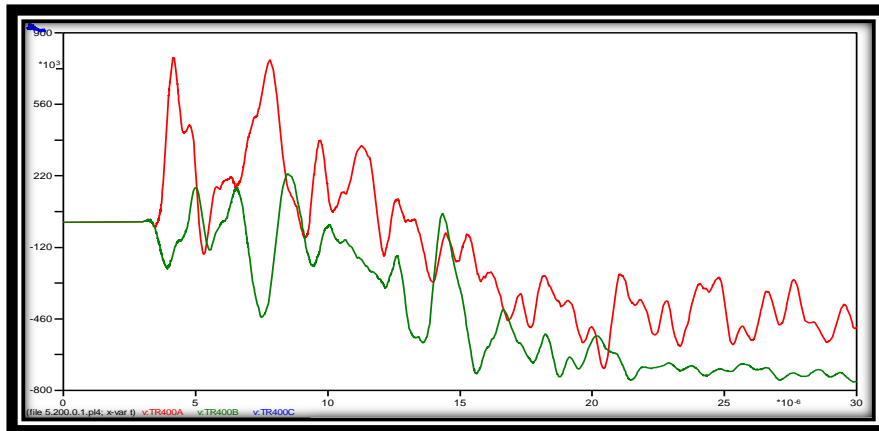


**Fig (4.3):** the transient over voltage on the primary winding of the transformer when distance( 5m) and the lightning current( 260 KA)

**Fig (4.4)** Shows the values of the internal voltages of the transformer the distance 10m the current is fixed using (Zinc Oxide PEXLIM –Q2).

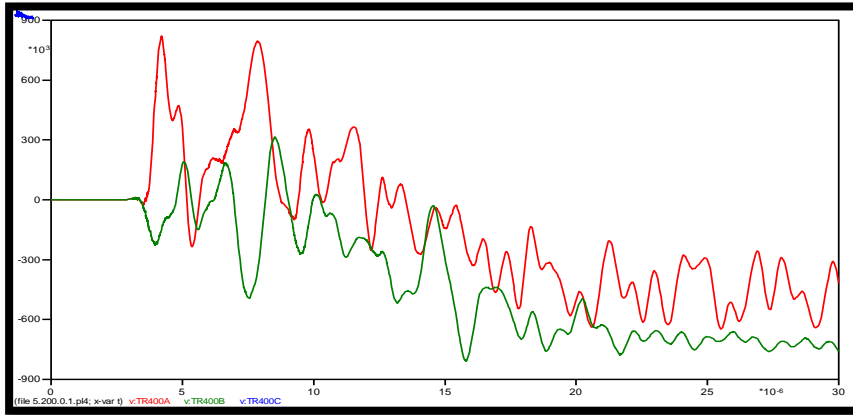


**Fig (4.4):** the transient over voltage on the primary winding of the transformer when distance( 10m) and the lightning current( 260 KA)

**Calculating the Basic Insulation level of the transformer (BIL):**

$$\%BIL = \frac{BIL - \text{max overvoltage}}{\text{max overvoltage}} \times 100$$

Where: (*BIL*) equal 1300kV[5].

(*max overvoltage*) Is the maximum voltage on the transformer on the primary side 400kV.To avoid destructive damage of the entire transformer the ratio of (*BIL*) must be more than 20% .

**4.1.1-Calculating (BIL) of the transformer when using both types table(4.5).**

**Table (4.5) Calculating (BIL) according to Effect of increasing the distance (the installation place of lightning arrester related to primary winding of the transformer) when the lightning current is fixed 260KA.**

Distance (m)	Zinc Oxide EXLIM – Q1		Zinc Oxide PEXLIM – Q2	
	Overtoltage (kV)	BIL%	Overtoltage (kV)	BIL%
5	894.17	45.23%	824.66	57.64%
10	994.88	30.66%	874.29	48.69%
15	1054.8	23.24%	904.08	43.79%
20	1097.9	18.42%	927.47	40.16%
25	1112.2	16.88%	940.02	38.29%
30	1134.7	14.56%	955.08	36.11%

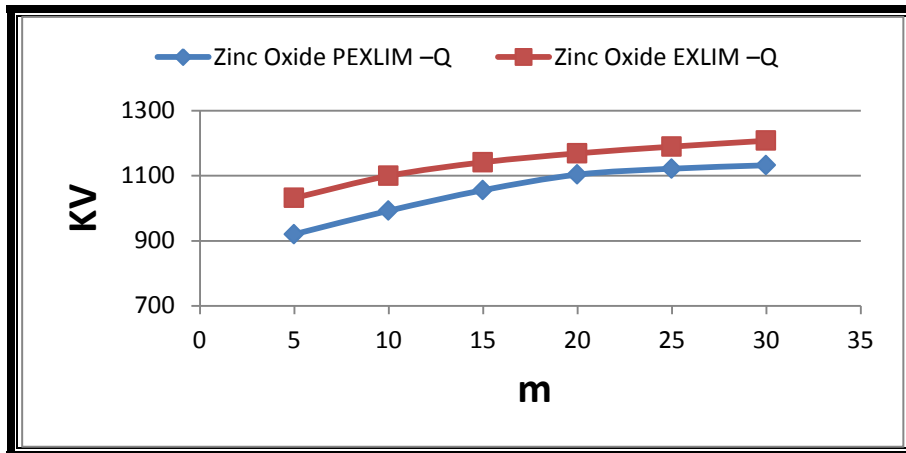


**Fig (4.6)-The effect of distance (the installation place of lightning arrester related to the transient over voltage on the primary winding) when the current is fixed 260KA. For both arresters**

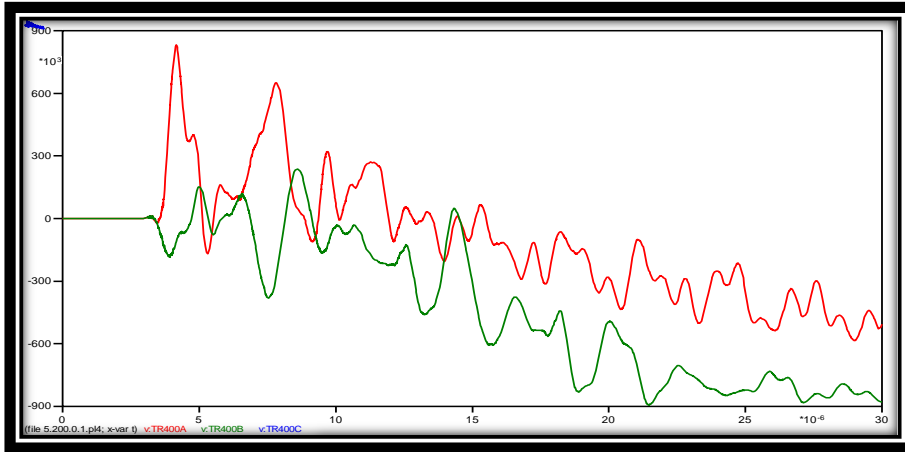
From the previous results it is clear that.

- The results in table (4.5) showed that as we increase the distance the internal transient over voltage increase and (BIL) is decreasing. and the decreasing is clear when the location of the arrester at 20 m (BIL) for(Zinc Oxide EXLIM- Q1) becomes less than the standard value (18.42%) compared with type (Zinc Oxide PEXLIM Q2)( 40.16%) .According to the value of (BIL) for both types the second one can stands the lightning stroke tell 30 m.
- Figure (4.6) shows the effect of increasing the distance in steps (the installation place of lightning arrester) related to the transient over voltage on the primary winding of the transformer when the lightning current is fixed 260KA. For both arresters of the arrester .according to table (4.5) as we increase the distance the voltage on the primary side of the transformer increasing. although both are increasing with the same range the transient over voltage on the (Zinc Oxide EXILIM – Q1) is higher compared with the voltages value of arrester (Zinc Oxide PEXLIM –Q2) and this makes the (BIL)decreases .quality 1=2

#### 4.2 - Second case:

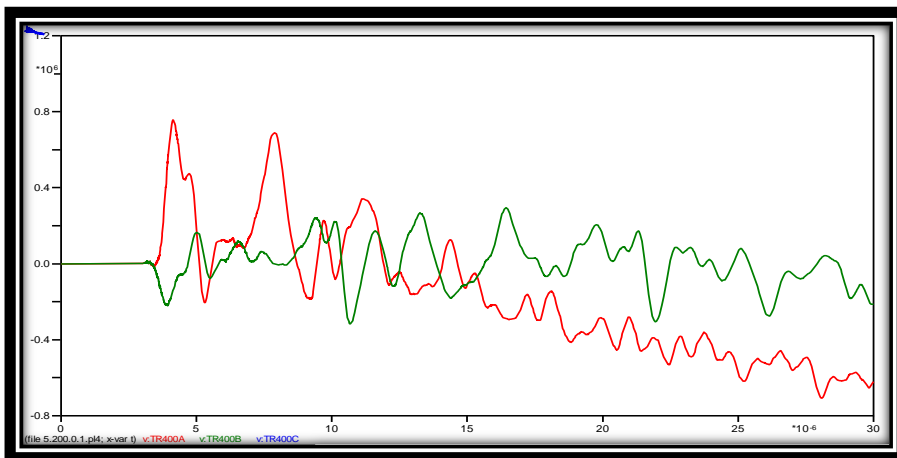
study the resulting the transient over voltage when the overhead ground wire exposed to lightning stroke the separation distance fixed to (5m) the lightning current strokes ranging from(260 to 300kA) increasing 10KA in each step using both arresters (Zinc Oxide PEXLIM –Q2) and (Zinc Oxide EXILIM –Q1).

Fig (4.7) shows the values of the internal transient over voltages of the transformer on the primary side 400kV changing the lightning current from (260 to 300kA) and distance is fixed 5m by using(Zinc Oxide EXILIM – Q1)..



**Fig (4.7): the transient over voltage on the primary winding of the transformer when distance (5m) and the lightning current (260 KA)**

**Figure (4.8)** shows the values of the internal voltages of the transformer when the lightning current is 260kA the distance is fixed 5m using (Zinc Oxide EXILIM-Q1).



**Fig (4.8): the transient over voltage on the primary winding of the transformer when distance (5m) and the lightning current (290 KA)**



**Figure (4.9)** Shows the values of the internal voltages of the transformer when the lightning current is 270kA the distance is fixed 5m using (Zinc Oxide PEXLIM–Q2).

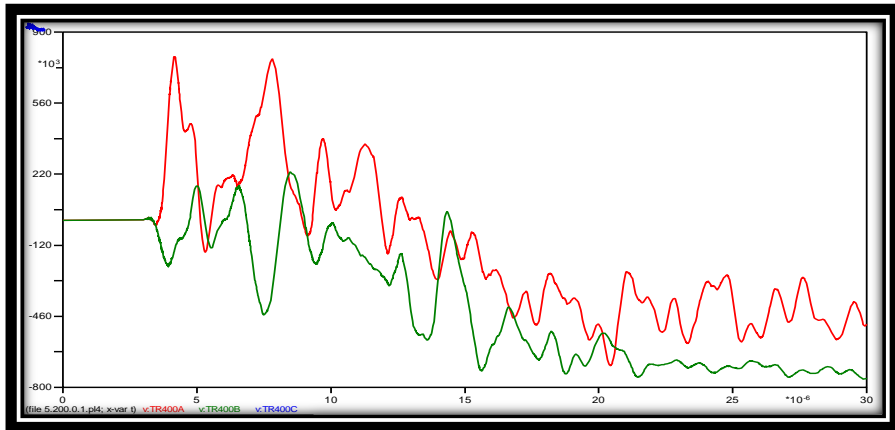


**Fig (4.9):** the transient over voltage on the primary winding of the transformer when distance (5m) and the lightning current (260 KA)

**Fig (4.10)** shows the values of the internal voltages of the transformer on the primary side 400kV result of lightning current 290kA by using (Zinc Oxide PEXLIM –Q2).

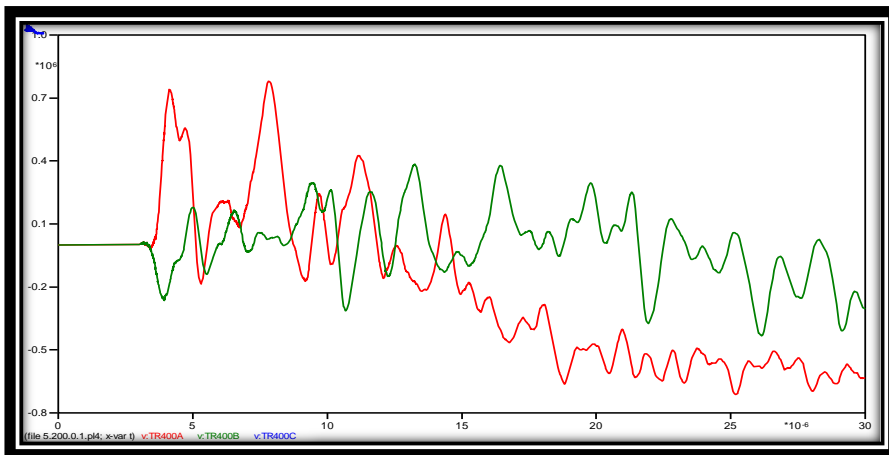


**Fig (4.10):** the transient over voltage on the primary winding of the transformer when distance (5m) and the lightning current (290 KA)

**4.2.1- Calculating the (BIL) of the transformer when using both types** when the separation distance is fixed (5m) and lightning current strikes ranging from(260 to 300kA)

The following table (4.6) shows the change of insulation level (BIL).

**Table (4.6) Calculating (BIL) according to Effect of increasing of lightning current and the distance (the installation place of lightning arrester related to primary winding of the transformer) is fixed to 5m**

Lightning current (kA)	Zinc Oxide EXILIM – Q1		Zinc Oxide PEXLIM – Q2	
	Overvoltage (kV)	BIL%	Overvoltage (kV)	BIL%
260	894.17	45.38%	824.66	57.46%
270	968.04	34.29%	877.48	48.15%
280	1017.2	27.80%	921.48	41.07%
290	1032.1	25.95%	933.32	39.28%
300	1036.6	22.22%	953.84	36.29%

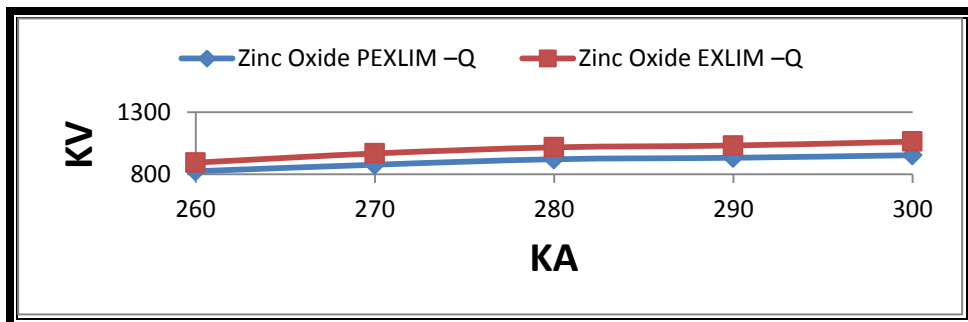


**Fig (4.11)-The effect of lightning current to the transient over voltage on the primary winding of transformer when the distance is fixed 5 m. For both arresters**

From previous results we can conclude the following:

- The results in table (4.6) show that as we increase the lightning current the internal transient over voltage increase and the (BIL) is decreasing it is clear when the lightning current is 300kA (BIL) for (**Zinc Oxide EXLIM- Q1**) is about to becomes less than the standard value (**22.22%**) compared with type (**Zinc Oxide PEXLIM Q2**)( **36.29%**) .according to the value of (BIL) for both types the second one can stands the lightning stroke better than the first one.
- Results in table (4.6) show that (BIL) decreasing as we increasing the current especially when the lightning current at 300KA and type (**Zinc Oxide PEXLIM Q2**). Stands much better than type (**Zinc Oxide EXLIM- Q1**) and the transformer will subjected to high voltage wave is about to break down and (BIL) stayed more than 20% even the lightning current at 300kA.
- Figure (4.11), as the arrester (the protection device) is close to transformer as the (BIL) is high even the current is high so by any way this means that distance factor is represented important role in protection المقاومة,while it finds that the value of the current in the arresters (**Zinc Oxide PEXLIM – Q2**) and (**Zinc Oxide EXILIM – Q1**) equally happen significant difference in voltage between retardants.

#### 4.3 -Third case:

3- Studying the voltage behavior when the lightning stroke falls direct to transmission line .When the lightning current ranging from (260kA to 300kA) And the separation distance fixed (5m) using both arresters.

**Fig(4.12)** shows the values of the internal transient over voltages of the transformer when the lightning strike transmission line directly the lightning current (300KA)and separation distance fixed (5m) by using (**Zinc Oxide EXILIM –Q1**).

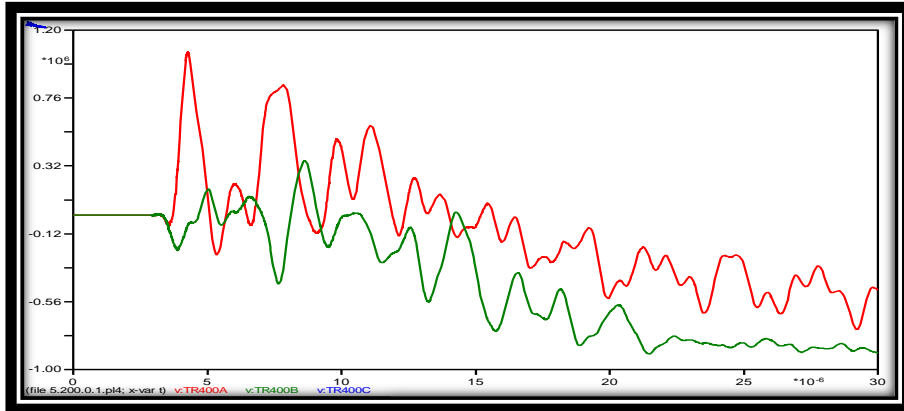


**Fig (4.12): the transient over voltage on the primary winding of the transformer when the lightning current (300kA) distance (5m)**

**Fig (4.13)** shows the values of the internal transient over voltages of the transformer when the lightning strike directly transmission line with lightning current (300KA) using (Zinc Oxide PEXLIM –Q2).

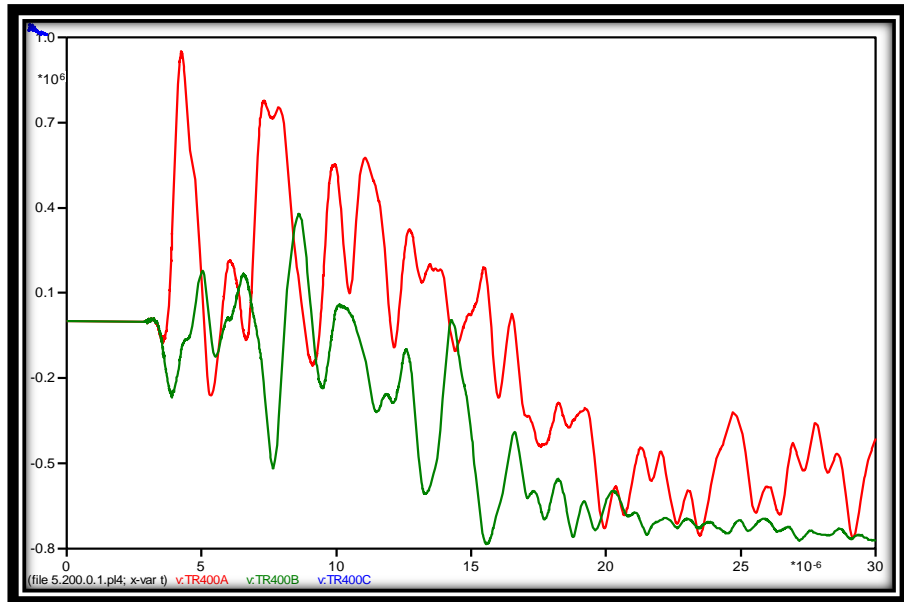


**Fig (4.13): the transient over voltage on the primary winding of the transformer when the lightning current (300kA) distance (5m)**

**4.3.1- Calculating the (BIL) of the transformer when using both types** when the separation distance is fixed (5m) and lightning current strikes ranging from(260 to 300kA)

The following table (4.7) shows the change of Basic insulation level (BIL).

**Table (4.7) Calculating (BIL) according to Effect of increasing the lightning current and the distance( the installation place of lightning arrester related to primary winding of the transformer) is fixed to 5 m. for both lightning arresters**

Lightning current (kA)	Zinc Oxide EXILIM – Q1		Zinc Oxide PEXLIM – Q2	
	Overvoltage (kV)	BIL%	Overvoltage (kV)	BIL%
260	1038.4	25.19%	943.67	%37.76
270	1039.2	25.09%	950.07	36.83%
280	1041.9	24.77%	5950.1	36.82%
290	1050.1	23.79%	950.20	36.81%
300	1057.9	22.88%	950.25	36.80%

**Note:** as we increase the lightning current by 10kA till 300kA as the basic insulation level (BIL) is decreasing for both arresters. according to the table (4.7) type (Zinc Oxide PEXLIM – Q2) can stands the lightning much better than type (Zinc Oxide EXILIM – Q1) which is about to Breakdown when the lightning current (300kA).

#### 4. Conclusions:

In this paper, a simple substation model and the effect of lightning strokes and a multiple strokes of lightning flash were all successfully simulated and analyzed using program ATP, and the effect of distance factor related to protection device was approved (place of lightning arrester).The study was supported with Different types of arresters which were identified and tested to choose the best one for power protection systems. More than this the results established the need for

lightning protection using lightning arresters .and results obtained by this study can summaries in these points:

- 1- As the separation distance between protection device (the installation place of the lightning arrester) and transformer increasing as the transient over voltage at the primary winding of the transformer increasing and (BIL) of the transformer decreasing compared to the standard level of (BIL) and the transformer will be more subjected to insulation failure .
- 2- As the current of lightning stroke increase as the transient over voltage on the primary winding of the transformer increasing. and the (BIL) will decrease then the transformer will be more subjected to damage
- 3- The separation distance and the lightning current are the main factors in our study the distance (the installation place of arrester related to the protected unit) is adjustable compared with lightning current is naturally uncontrollable and because Most of the transformers failures seem to be due to the excessive separation lengths between the transformer and the lightning arresters which will expose the transformer to excessive transient over voltage so it should always be evaluated to ensure adequate protection.
- 4- Point (1) and (2) according to the results for (BIL) transient overvoltage approving that the priority is for the distance (location of the lightning arrester related to transformer) then the value of the current of lightning stroke comparing two different tests. Distance factor is playing the important role in protection even the lightning current is very high.
- 5- Two types of lightning arresters were tested(**Zinc Oxide PEXLIM Q2**) and(**Zinc Oxide EXLIM- Q1**) and results approved that (**Zinc Oxide PEXLIM Q2**) is much better than the first one for withstanding traveling waves due to lightning which causing insulation failure in power systems.

## 5. References

- [1] GREENWOOD, A. *Electrical Transients in Power Systems*. New York: John Wiley & Sons, 1991. ISBN 978-0471620587
- [2] S. Furukawa, O. Usuda, T. Isozaki, and T. Irie, "Development and application of lightning arresters for transmission lines," *IEEE Trans. PowerDel.*, vol. 4, no. 4, pp. 2121–2129, Oct. 1999.
- [3] R. E. Koch, J. A. Timoshenko, J. G. Anderson, and C. H. Shih, "Design of zinc oxide transmission line arresters for application on 138

- [4] kV towers,” *IEEE Trans. Power App. Syst.*, vol. PAS-104, no. 10, pp.2675–2680, Oct. 1985.
- [5] J. L. He, R. Zeng, S. M. Chen, and Y. P. Tu, “Thermal characteristics of high voltage whole-solid-insulated polymeric ZnO surge arrester,” *IEEETrans. Power Del.*, vol. 18, no. 3, pp. 1221–1227, Jul. 2003.
- [6] R. E. Koch, J. A. Timoshenko, J. G. Anderson, and C. H. Shih, “Design of zinc oxide transmission line arresters for application on 138
- [7] kV towers,” *IEEE Trans. Power App. Syst.*, vol. PAS-104, no. 10, pp.2675–2680, Oct. 1985.
- [8] [www.arresterworks.com](http://www.arresterworks.com).

## Reversible Blind Image Watermarking based on Integer Wavelet Transform

Abdulmawla Najih<sup>1</sup>, Salem Enajeh<sup>2</sup>, Nabila Albannai<sup>3</sup>

<sup>1,2</sup>Department of computer engineering, The High Institute of Science & Technology Gharian

<sup>3</sup>Department of computer engineering, The High Institute of Science & Technology Tripoli

nabdulmawla@gmail.com<sup>1</sup> , alnaghsa@gmail.com<sup>2</sup> ,  
rehamranemrahf2009@gmail.com<sup>3</sup>

### المخلص:

في هذا البحث، تم اقتراح تقنية جديدة للعلامة المائية الرقمية لتضمينها داخل الصورة باستخدام التحويل المويجي الصحيح (IWT) تم تطوير تقنية العلامة المائية الرقمية وذلك لاسخدامها في بعض التطبيقات مثل التعرف على الوجوه التي تتطلب صورة عالية الجودة ليكون الأداء افضل الأداء. لهذا الهدف، يتم تطبيق IWT على الصورة لتحليلها إلى نطاقات فرعية مختلفة. اعتماداً على القوة المرغوبة للعلامة المائية، يتم تحديد النطاق الفرعي للموجة. وبالتالي، يتم تضمين العلامة المائية في زوج من قيم المويجات. أخيراً، يتم إعادة بناء الصورة ذات العلامة المائية من خلال تطبيق IWT المعكوس. حيث يتم استخراج بيانات العلامة المائية من الصورة المتضمنة العلامة المائية. بعد ذلك، يتم استعادة الصورة الأصلية باستخدام العلامة المائية المستخرجة. النتائج العملية أثبتت أن تقنية العلامة المائية المقترحة لا تتمتع فقط بقوة اخفاء البيانات ولكن لديها أيضاً القدرة على كمية بيانات كبيرة.

الكلمات المفتاحية: العلامات المائية للصورة الرقمية، العلامة المائية القابلة للانعكاس، التحويل المويجي الصحيح، العلامة المائية العمياء، العلامة المائية العكسية.

### Abstract:

In this paper a new reversible (also known as invertible) blind image watermarking technique is proposed based on Integer Wavelet Transform (IWT). This lossless image watermarking technique is developed for some applications like face recognition that a high perceptual quality image is required in order to preserve the performance. For this aim, IWT is applied on an image to decompose it to different sub-bands. Depending on the desired robustness of the watermark, the wavelet's sub-band is selected. Thus, a lossless function is used to embed the watermark into pair of wavelet's values. Finally, watermarked image is



reconstructed by applying inverse IWT. At receiver side, watermark data is extracted from the watermarked image. Then, the original image is recovered by using extracted watermark. Experimental results reveal that the proposed watermark technique not only has proper invisibility but also it has high payload.

**Keywords:** Digital image watermarking, reversible watermark, integer wavelet transform, blind watermark, invertible watermark.

## 1. Introduction

Nowadays, there is special attention to digital watermarking due to its wide applications such as fingerprinting, copyright control and protection, authentication, etc. Embedding extra information into the original content makes a slight difference between original content and watermarked content. Majority of the available watermarking techniques are irreversible which the original content cannot be recovered [1]. Distribution and transmission the watermarked version cannot be always acceptable by some applications such as biometric recognition [2], military investigation, space exploration, and medical diagnosis. In these applications, the security of the content as well as quality of the content must be satisfied. Thus, another kind of watermarking known as reversible watermarking is applied to satisfy both of them. Reversible (or also called lossless or invertible) watermarking does not have any degradation on original content [3]. All of the reversible watermarking are fragile or semi-fragile which can easily be destroyed if any modification is taken place [4]. Figure 1 illustrates two major categories of reversible watermarking techniques.

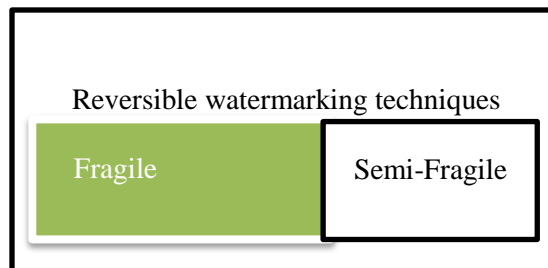


**Figure 1. Two main classes in reversible image watermarking techniques.**

In this paper, a novel reversible image watermarking technique is proposed by using IWT. The main reason is the ability of IWT for transforming an image to some sets of integer. Furthermore, applying lossless functions for watermark embedding and watermark extraction are broadening the application of this technique for wide range of applications.

The rest of this paper is organized as follow: first, related works in reversible image watermarking are discussed; second, the proposed reversible image watermarking technique is explained; third, an experimental result on the proposed reversible image watermarking technique is provided; fourth, the proposed algorithm is compare with other techniques; and finally, conclusions and future trends are presented.

## 2. Related Works

Majority of reversible image watermarking techniques have been classified into two main techniques including semi-fragile and fragile watermarking techniques. Figure 2 presents available reversible image watermarking techniques.

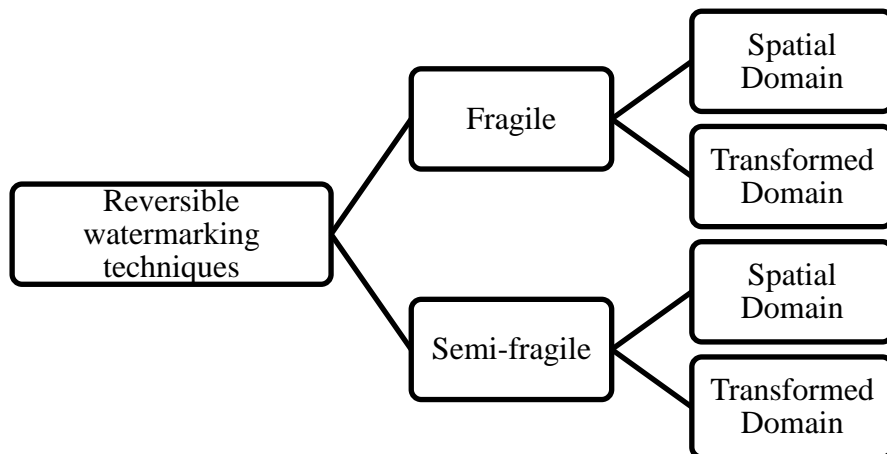


Figure 2. Available techniques for reversible image watermarking techniques.

Fragile reversible image watermarking based on spatial domain: The first technique for fragile reversible image watermarking has been presented based on differences among the neighborhoods pixels [5]. Although this technique can provide high amount of payload, the invisibility of the watermark can be degraded.

Fragile reversible image watermarking based on transform domain: A technique has been developed that apply a transformation functions like DCT in order to embed the watermarking bit bases on ZRX (Zero-Replacement Extraction), CA (Confusion Avoidance), or ZRE (Zero-Replacement Embedding) [6]. Although this technique can provide reasonable watermark invisibility, the low embedding capacity is the main problem of this approach. Another algorithm has been used based on substitution scheme for color images watermarking using Fourier transform [7]. Although the low capacity is the main issue of this study.

Semi-fragile reversible image watermarking based on spatial domain: A investigation has been developed based on modifying histograms of two sets [8]. For this purpose, two sets of regions in the image are selected. Then, watermark bit is inserted by changing the histograms' bins.

Semi-fragile reversible image watermarking based on transform domain: A study in [9] has been developed based on Weighted Quantization Method (WQM) by using two functions such as F and L. L is consisted of different quantization steps but F is the main quantization function. Another method has been presented based on LBP operators by using the local pixel contrast for the embedding and extraction of watermarks [10]. However, this technique can provide high amount of payload, the invisibility of the watermark can be degraded.

### **3. Proposed Watermarking Algorithm**

Apart from watermark types, every watermarking algorithm has two common aspects including watermark embedding and watermark extraction. In the following, both of these aspects are explained in the details.

#### **3.1 Watermark Embedding**

The watermark embedding process is described as following:

- 1- Read the original image from input.
- 2- Apply one level two dimensional IWT on original image to decompose it four sub-bands including  $cA$ ,  $cH$ ,  $cV$ , and  $cD$ .
- 3- Rearrange details coefficients of the wavelet ( $cD$ ) to a matrix with size of  $2 \times N$  ( $A_{2 \times N}$ ).
- 4- For each watermark bit, select pair of values ( $X$ ,  $Y$ ) from  $A_{2 \times N}$ .
- 5- Compute the amount of  $L$  and  $H$  based on equation (1):

$$L = \left\lfloor \frac{X+Y}{2} \right\rfloor, \quad H = X - Y \quad (1)$$

- 6- Check the condition as in Equation (2)
- 7- Embed the binary watermark ( $W_i$ ) data as in Equation (3):

$$\hat{H} = 2H + W_i \quad (3)$$

- 8- Compute the modified amount as in Equation (4):

$$\hat{X} = L + \left\lfloor \frac{\hat{H}+1}{2} \right\rfloor, \quad \hat{Y} = L - \left\lfloor \frac{\hat{H}}{2} \right\rfloor \quad (4)$$

Reconstructed the modified wavelet's details coefficients ( $\widehat{cD}$ ) from the modified matrix ( $\widehat{A_{2 \times N}}$ ).

- 9- Replace  $\widehat{cD}$  instead of  $cD$  and apply inverse one level two dimensional IWT to reconstruct the watermarked image.

### 3.2 Watermark Extraction

The watermark extraction process is described as following:

- 1- Read the watermarked image from input.
- 2- Apply one level two dimensional IWT on watermarked image to decompose it four sub-bands including  $cA$ ,  $cH$ ,  $cV$ , and  $cD$ .
- 3- Rearrange details coefficients of the wavelet ( $cD$ ) to a matrix with size of  $2 \times N$  ( $A_{2 \times N}$ ).
- 4- For each watermark bit, select pair of values ( $X$ ,  $Y$ ) from  $A_{2 \times N}$ .
- 5- Compute the amount of  $\widehat{L}_{org}$  and  $\hat{H}$  based on equation (5):

$$\widehat{L}_{org} = \left\lfloor \frac{\hat{X}+\hat{Y}}{2} \right\rfloor, \quad \hat{H} = \hat{X} - \hat{Y} \quad (5)$$

- 6- Extract the binary watermark ( $\widehat{W}_i$ ) data as in Equation (6):

$$\widehat{W}_i = \widehat{H}_{org} \% 2 \quad (6)$$

7- Compute the new amount of  $\widehat{H}$  before watermarking as in Equation (7)

$$\widehat{H}_{org} = \frac{\widehat{H} - \widehat{W}_i}{2} \quad (7)$$

8- Compute the original amount of image as in Equation (8):

$$\widehat{X}_{org} = \widehat{L}_{org} + \left\lfloor \frac{\widehat{H}_{org} + 1}{2} \right\rfloor, \quad \widehat{Y}_{org} = \widehat{L}_{org} - \left\lfloor \frac{\widehat{H}_{org}}{2} \right\rfloor \quad (8)$$

9- Reconstructed the modified wavelet's details coefficients ( $\widehat{cD}$ ) from the modified matrix ( $\widehat{A}_{2 \times N}$ ).

10- Replace  $\widehat{cD}$  instead of  $cD$  and apply inverse one level two dimensional IWT to reconstruct the original image.

In order to describe the proposed algorithm more clearly, Figure 3 presents the pseudocode for watermark embedding and extraction processes.











**Img**: input image  
**Img\_wm**: watermarked image  
**Img\_org**: constructed original image from the watermarked image  
**cA, cH, cV, cD**: wavelet coefficients  
**N**: size of cD  
**A**: Revised matrix from cD  
**BB**: Modified matrix  
**Floor()**: floor function  
**Reshape()**: matrix reshaping function  
**IWT()**: Integer wavelet transform function  
**Inverse LWT**: Inverse integer wavelet transform function  
**Min**: find minimum among between two values

<ol style="list-style-type: none"> <li>1. Read original image (img) from input.</li> <li>2. [cA cH cV cD]=IWT(img).</li> <li>3. A = reshape(cD,2,N);</li> <li>4. For i=1:N                  x=B(1,i).                  y=B(2,i).                  l=floor((x+y)/2).                  h=x-y.</li> <li>5. If abs(2*h+ wi)&lt;=min(2(255-1),2*l+1)                  hh=2*h+w<sub>i</sub>.                  xx=1+floor((hh+1)/2).                  yy=1-floor(hh/2).                  B(1,i)=xx.                  B(2,i)=yy.</li> <li>6. End of If</li> <li>7. End of for</li> <li>8. AA = reshape(B).</li> <li>9. img_wm =inverse IWT(cA,cH,cV,AA).</li> </ol>	<ol style="list-style-type: none"> <li>1. Read watermarked image (img_wm) from input.</li> <li>2. [cA cH cV cD]=IWT(img_wm).</li> <li>3. A = reshape(cD,2,N);</li> <li>4. For i=1:N                  xx=B(1,i);                  yy=B(2,i);                  lll=floor((xx+yy)/2);                  hhh=xx-yy;                  ww<sub>i</sub>= mod(double(hhh), 2);                  h_real=(hhh-ww(i))/2;                  xx=lll+floor((h_real+1)/2);                  yy=lll-floor(h_real/2);                  BB(1,i)=xx;                  BB(2,i)=yy;</li> <li>5. End</li> <li>6. BBB = reshape(BB);</li> <li>7. img_org= inverse IWT(cA,cH,cV,BBB,liftscheme);</li> </ol>
---	--

**Figure 3. Pseudocode for the proposed embedding and extraction processes**

#### 4. Experimental Results

In this part, the performance of the proposed invertible image watermarking technique based on IWT is evaluated. For this purpose, five images were selected including Lena, baboon, cameraman, Barbara,

				
(a)	(b)	(c)	(d)	(e)
				
(f)	(g)	(h)	(i)	(j)
39.53 dB	41.01 dB	40.55 dB	42.44 dB	40.43 dB

**Figure 4. Original images of (a) Lena (b) baboon (c) cameraman (d) Barbara (e) pepper and the watermarked images of (f) Lena (g) baboon (h) cameraman (i) Barbara (j) pepper.**

Table 1 presents the major criterion for the proposed image watermarking technique. As seen, the invisibility and capacity can fully meet. However, due to fragility nature of the proposed reversible watermarking technique, the watermark data always extracted with random nature.

**Table 1. various watermarking factors for the developed image watermarking technique.**

Image	PSNR (dB)	Capacity (b)	Avr BER (%)
Lena	39.53	6272	49

Baboon	41.01	6272	44
Cameraman	40.55	6272	54
Barbara	42.44	6272	59
Pepper	40.43	6272	55

Table 2 presents amount of different criterion for the developed reversible image watermarking technique. As seen, Mean Square Error (MSE) revealed that when there was no attack, the constructed images were exactly similar to original images. In addition, the amount of Peak to Signal Noise Ratio (PSNR) between original and constructed images were infinity which show perfect recovered images. However, under attacks, the proposed reversible image watermarking was behaved like fragile which can be inferred from the amount of Bit Error Rate (BER). Apart from these criterion, it can easily infer that the reversible image watermark is only applying for environment without any attack.

Table 2. Different factors for the developed reversible image watermarking technique.

Attack	MSE	BER	PSNR
No attack	0	0	$\infty$
Salt and pepper noise	1.2397e+04	43	29.54
AWGN	1.1586e+04	45	23.23
JPEG	1.2386e+04	62	31.43
Rotation and scaling	1.2586e+04	23	33.34
Cutting	1.2576e+04	33	24.54
Filter	1.0126e+04	51	26.65



## 5. Discussion

Digital image watermarking induces undesired noise into the image. Therefore, some applications like face recognition cannot use

watermarking technology for its security. Although image enhancement techniques may have some improvements for the performance of face recognition for noisy face images, the facial and other important components of the image also be affected. Therefore, developing invertible image watermarking for these types of applications is required. In this paper, a novel invertible image watermarking technique is proposed that not only can carry the watermark but also, the original image can be retrieve from the watermarked image blindly. This algorithm can support multimodal biometric systems that are based on facial and watermarked data. For this purpose, fingerprint biometric information is embedded as a watermark data which is not degrade the facial biometric information due to invertibility feature in the nature of the proposed watermark.

## 6. Conclusions and Future Trends

This paper has been discussed the reversible image watermarking framework which is based on IWT and some reversible functions. To achieve this aim, couple of pixels have been used to carry the watermark data. Although watermarking can provide reasonable watermark's capacity and invisibility, it may degrade under intentional and unintentional attacks. Experimental results reveal that the proposed algorithm can properly compute the original image from the watermarked image when no attacks are taken place. Future trends in this work can be apply other transformation techniques such as DCT, FFT, and multi-resolution transformation to improve watermark invisibility and improve capacity.

## References

- [1]Y. Luo *et al.*, "A multi-scale image watermarking based on integer wavelet transform and singular value decomposition," *Expert Systems with Applications*, vol. 168, p. 114272, 2021.
- [2] A. Najih, S. Alhaddad, S. Hashim, and N. Albannai, "Matching Face Images for Biometric Authentication," in *2019 IEEE Conference on*

- Sustainable Utilization and Development in Engineering and Technologies (CSUDET)*, 2019: IEEE, pp. 34-38.
- [3]N. M. Makbol, B. E. Khoo, T. H. Rassem, and K. Loukhaoukha, "A new reliable optimized image watermarking scheme based on the integer wavelet transform and singular value decomposition for copyright protection," *Information Sciences*, vol. 417, pp. 381-400, 2017.
- [4]R. Caldelli, F. Filippini, and R. Becarelli, "Reversible watermarking techniques: an overview and a classification," *EURASIP Journal on Information Security*, vol. 2010, no. 1, p. 1, 2010.
- [5]J. Tian, "Reversible data embedding using a difference expansion," *IEEE Trans. Circuits Syst. Video Techn.*, vol. 13, no. 8, pp. 890-896, 2003.
- [6] C.-C. Chen and D.-S. Kao, "DCT-based reversible image watermarking approach," in *Intelligent Information Hiding and Multimedia Signal Processing, 2007. IHHMSP 2007. Third International Conference on*, 2007, vol. 2: IEEE, pp. 489-492.
- [7]K. Fares, K. Amine, and E. Salah, "A robust blind color image watermarking based on Fourier transform domain," *Optik*, vol. 208, p. 164562, 2020.
- [8] E. Chrysochos, V. Fotopoulos, A. Skodras, and M. Xenos, "Reversible image watermarking based on histogram modification," in *Proc. 11th Panhellenic Conf. Informatics (PCI 2007)*, 2007, pp. 93-104.
- [9] M. J. Saberian, M. A. Akhaee, and F. Marvasti, "An invertible quantization based watermarking approach," in *2008 IEEE International Conference on Acoustics, Speech and Signal Processing*, 2008: IEEE, pp. 1677-1680.
- [10]Z. Wenyin and F. Y. Shih, "Semi-fragile spatial watermarking based on local binary pattern operators," *Optics Communications*, vol. 284, no. 16-17, pp. 3904-3912, 2011.